upregulation of *Gata3* is mediated through direct transactivation by Lhx2. However, Lhx2 N-finger point mutants (mtLIM-C, mtLIM-NC) exhibited a weaker activity for the expansion of c-Kit$^+$ cells despite having a normal transcription factor activity. Therefore, it is likely that the upregulation of *Gata3* is an indirect event. Since our data suggest that Lmo2 can regulate *Gata3* expression, the degradation of Lmo2 might result in the upregulation of *Gata3*. In fact, overexpression of Lmo2 attenuated the Lhx2-mediated upregulation of *Gata3* mRNA (Fig. 5G). These findings uncovered a novel molecular pathway underlying the Lhx2-induced expansion of KSL/KL cells. Notably, microarray data revealed that *hprt1/hprt* was upregulated by Lhx2 (Supporting Information Table S2A). In iLhx2-ESCs, dox-inducible Lhx2 expression cassette was located in the *hprt1/hprt* locus. Hence, it might be possible that dox addition would activate the adjacent *hprt1/hprt* gene. However, in ESCs, it was not the case (Supporting Information Fig. S4A). Therefore, expression of *hprt1/hprt* is not influenced by tetracycline responsive elements itself. In contrast, in the Lhx2-induced KSL/KL cells, *hprt1/hprt* expression was decreased by withdrawal of dox (Supporting Information Fig. S4B). Thus, *hprt1/hprt* could be one of the Lhx2-target genes in these cell population.

In the mouse embryonic brain, Lhx2 is expressed in cortical precursor cells and operates as a selector gene to maintain cell identity [27]. This data revealed that Lhx2 maintains KSL/KL cell identity, and it is likely that these two effects of Lhx2 are mediated by a common mechanism. Lhx2 interacts with MRG1/Cited2 [28], which associates with the histone acetyltransferase CBP/p300. Thus, the ability of Lhx2 to maintain the identities of KSL/KL cells and cortical precursor cells might be dependent on epigenetic control mediated by these nuclear factors.

Several LIM-HD and Lmo proteins competitively associate with Ldb, and these interactions appear to regulate a variety of biological events in vertebrates and invertebrates. In *Drosophila*, the *Lhx2* homolog *Apterous* is required to specify dorsal cell fate during wing disc formation, and the activity of Apterous in this compartment depends on Chip, an Ldb protein in *Drosophila* [29]. Apterous activity is regulated by the Lmo protein, dLmo [30]. In chick limb development, inhibition of Lhx2 activity arrests limb outgrowth, and CLIM2/Ldb1 inhibition results in the same phenotype [22, 31, 32]. Thus, regulation of transcription factor complexes comprising LIM-HD, Ldb, and Lmo seems to be important for embryonic development of various organisms. Degradation of Lmo2 is mediated by the E3 ubiquitin ligase Rlim/Rnf12 [23]. Rlim/Rnf12 also induces Ldb1 degradation [23], suggesting that Rlim/Rnf12 regulates the abundance of Lmo2 and Ldb1, and that the maintenance of these cofactors at appropriate levels is important for coordinated developmental processes. Recently, it was demonstrated that *Rlim/Rnf12* controls neural induction and mesoderm formation from ESCs [33], suggesting this molecule has indispensable roles in embryonic development.

A transcription factor complex comprising Lmo2, Tal1/Scl, Gata1, Ldb1, and E47 regulates erythroid-specific gene expression [34]. *Lmo2*-null mice die in utero due to failure of yolk sac primitive erythropoiesis. This suggests that Lmo2 plays an important role in the induction of erythroid differentiation. Moreover, Lmo2 is also required for definitive hematopoiesis [35, 36]. *Lmo2*-null ESCs do not contribute to any lineages of adult hematopoietic cells in chimeric mice in vivo [36], suggesting that Lmo2 is required for lineage differentiation of HSCs/HPCs. It remains to be determined whether Lmo2 is also involved in the self-renewal and/or survival of HSCs. Interestingly, Lmo2 overexpression increased the frequency of Lin$^+$ cells in the Lhx2-induced KSL/KL cells when we used Gata1^{KO} ESCs (Supporting Information Fig. S2D). This suggests that Gata1 is dispensable for Lmo2 function in this context.

Gata2 and Gata3 can associate with Lmo2 [23, 37]. Therefore, Lmo2 may function in HSCs by associating with Gata2 and/or Gata3. Interestingly, an association partner of Lmo2, Tal1/Scl, is required for yolk sac primitive erythropoiesis and definitive hematopoiesis [25, 26]. The phenotypes of *Lmo2*-null and *Tal1/Scl*-null embryos are indistinguishable. Therefore, Lmo2 and Tal1/Scl may work together in HSCs. Surprisingly, when the *Tal1/Scl* gene was conditionally deleted in adult HSCs using the Cre/LoxP system, the HSCs retained LTR activity [38]. Thus, Tal1/Scl is required for HSC development but not for the maintenance of HSCs in adulthood. Presumably, Lmo2 may also be dispensable in the adult HSC compartment.

When *Tal1/Scl* is transduced into adult HSCs, the HSCs preferentially differentiate into myeloid cells [39]. Our data revealed that transduction of *Lmo2* into the Lhx2-induced KSL/KL cells resulted in differentiation into Mac-1$^+$ myeloid cells. It is likely that this is due to an excess amount of the transcriptional complex comprising Lmo2, Tal1/Scl, and possibly Ldb1.

Our previous transplantation assay and present in vitro differentiation experiments suggest that Lhx2 inhibits T-cell differentiation [14]. Aberrant *Lmo2* expression due to chromosomal translocation is one of the major causes of acute T-cell leukemia [40]. Although the role of Lmo2 and other Lmo family members in normal T-cell development remains obscure, Lhx2-mediated inhibition of T-cell differentiation might be explained by the decreased availability of Lmo2 and/or other Lmo proteins.

Conclusion

Using a conditional gene expression system in ESCs, we revealed that robust production of KSL/KL cells from ESCs by the enforced expression of Lhx2 was caused by quantitative changes in the levels of transcription factors and cofactors critical for embryonic hematopoiesis. Our findings are helpful for the application of Lhx2, and Lhx2-interacting molecules identified in this study, in the induction of HSCs/HPCs from human iPS cells.

Acknowledgments

This work was supported by Grants-in-Aid for Scientific Research from the Ministry of Education, Culture, Sports, Science, and Technology of Japan (24591415 to K.K. and 23390256 to K.K. and T.H.), and the SENSHIN Medical Research Foundation.

Disclosure of Potential Conflicts of Interest

The authors indicate no potential conflicts of interest.

REFERENCES

1 Metcalf D. On hematopoietic stem cell fate. Immunity 2007;26:669–673.
2 Oh IH, Humphries RK. Concise review: Multidimensional regulation of the hematopoietic stem cell state. Stem Cells 2012;30:82–88.
3 Shivdasani RA, Orkin SH. The transcriptional control of hematopoiesis. Blood 1996;87:4025–4039.
4 Cedar H, Bergman Y. Epigenetics of haematopoietic cell development. Nat Rev Immunol 2011;11:478–488.
5 Hobert O, Westphal H. Functions of LIM-homeobox genes. Trends Genet 2000;16:75–83.
6 Matthews JM, Bhati M, Craig VJ et al. Competition between LIM-binding domains. Biochem Soc Trans 2008;36:1393–1397.
7 Bach I, Rhodes SJ, Pearse RV et al. P-Lim, a LIM homeodomain factor, is expressed during pituitary organ and cell commitment and synergizes with Pit-1. Proc Natl Acad Sci USA 1995;92:2720–2724.
8 Xu Y, Baldassare M, Fisher P et al. LH-2: A LIM/homeodomain gene expressed in developing lymphocytes and neural cells. Proc Natl Acad Sci USA 1993;90:227–231.
9 Porter FD, Drago J, Xu Y et al. Lhx2, a LIM homeobox gene, is required for eye, forebrain, and definitive erythrocyte development. Development 1997;124:2935–2944.
10 Rhee H, Polak L, Fuchs E. Lhx2 maintains stem cell character in hair follicles. Science 2006;312:1946–1949.
11 Al-Jehani F, Hochhaus A, Spencer A et al. Expression of the LH2 gene in chronic myeloid leukaemia cells. Leukemia 1996;10:1122–1126.
12 Pinto do OP, Richter K, Carlsson L. Hematopoietic progenitor/stem cells immortalized by Lhx2 generate functional hematopoietic cells in vivo. Blood 2002;99:3939–3946.
13 Pinto do OP, Kolterud A, Carlsson L. Expression of the LIM-homeobox gene LH2 generates immortalized steel factor-dependent multipotent hematopoietic precursors. EMBO J 1998;17:5744–5756.
14 Kitajima K, Minehata K, Sakimura K et al. In vitro generation of HSC-like cells from murine ESCs/iPSCs by enforced expression of LIM-homeobox transcription factor Lhx2. Blood 2011;117:3748–3758.
15 Manaia A, Lemarchandel V, Klaine M et al. Lmo2 and GATA-3 associated expression in intraembryonic hemogenic sites. Development 2000;127:643–653.
16 Kitajima K, Zheng J, Yen H et al. Multipotential differentiation ability of GATA-1-null erythroid-committed cells. Genes Dev 2006;20:654–659.
17 Iacovino M, Bosnakovski D, Fey H et al. Inducible cassette exchange: A rapid and efficient system enabling conditional gene expression in embryonic stem and primary cells. Stem Cells 2011;29:1580–1588.
18 Kitajima K, Tanaka M, Zheng J et al. In vitro differentiation of mouse embryonic stem cells to hematopoietic cells on an OP9 stromal cell monolayer. Methods Enzymol 2003;365:72–83.
19 Wiznerowicz M, Trono D. Conditional suppression of cellular genes: Lentivirus vector-mediated drug-inducible RNA interference. J Virol 2003;77:8957–8961.
20 Kitajima K, Masuhara M, Era T et al. GATA-2 and GATA-2/ER display opposing activities in the development and differentiation of blood progenitors. EMBO J 2002;21:3060–3069.
21 Richter K, Wirta V, Dahl L et al. Global gene expression analyses of hematopoietic stem cell-like cell lines with inducible Lhx2 expression. BMC Genomics 2006;7:75.
22 Bach I, Rodriguez-Esteban C, Carriére C et al. RLIM inhibits functional activity of LIM homeodomain transcription factors via recruitment of the histone deacetylase complex. Nat Genet 1999;22:394–399.
23 Ostendorff HP, Peirano RI, Peters MA et al. Ubiquitination-dependent cofactor exchange on LIM homeodomain transcription factors. Nature 2002;416:99–103.
24 Akashi K, Traver D, Miyamoto T et al. A clonogenic common myeloid progenitor that gives rise to all myeloid lineages. Nature 2000;404:193–197.
25 Porcher C, Swat W, Rockwell K et al. The T cell leukemia oncoprotein SCL/tal-1 is essential for development of all hematopoietic lineages. Cell 1996;86:47–57.
26 Shivdasani RA, Mayer EL, Orkin SH. Absence of blood formation in mice lacking the T-cell leukaemia oncoprotein tal-1/SCL. Nature 1995;373:432–434.
27 Mangale VS, Hirokawa KE, Satyaki PR et al. Lhx2 selector activity specifies cortical identity and suppresses hippocampal organizer fate. Science 2008;319:304–309.
28 Glenn DJ, Maurer RA. MRG1 binds to the LIM domain of Lhx2 and may function as a coactivator to stimulate glycoprotein hormone alpha-subunit gene expression. J Biol Chem 1999;274:36159–36167.
29 Ghazi A, Anant S, VijayRaghavan K. Apterous mediates development of direct flight muscles autonomously and indirect flight muscles through epidermal cues. Development 2000;127:5309–5318.
30 Weihe U, Milán M, Cohen SM. Regulation of Apterous activity in Drosophila wing development. Development 2001;128:4615–4622.
31 van Meyel DJ, O'Keefe DD, Jurata LW et al. Chip and apterous physically interact to form a functional complex during Drosophila development. Mol Cell 1999;4:259–265.
32 Milán M, Cohen SM. Regulation of LIM homeodomain activity in vivo: A tetramer of dLDB and apterous confers activity and capacity for regulation by dLMO. Mol Cell 1999;4:267–273.
33 Zhang L, Huang H, Zhou F et al. RNF12 controls embryonic stem cell fate and morphogenesis in zebrafish embryos by targeting Smad7 for degradation. Mol Cell 2012;46:650–661.
34 Wadman IA, Osada H, Grütz GG et al. The LIM-only protein Lmo2 is a bridging molecule assembling an erythroid, DNA-binding complex which includes the TAL1, E47, GATA-1 and Ldb1/NLI proteins. EMBO J 1997;16:3145–3157.
35 Warren AJ, Colledge WH, Carlton MB et al. The oncogenic cysteine-rich LIM domain protein rbtn2 is essential for erythroid development. Cell 1994;78:45–57.
36 Yamada Y, Warren AJ, Dobson C et al. The T cell leukemia LIM protein Lmo2 is necessary for adult mouse hematopoiesis. Proc Natl Acad Sci USA 1998;95:3890–3895.
37 Ono Y, Fukuhara N, Yoshie O. TAL1 and LIM-only proteins synergistically induce retinaldehyde dehydrogenase 2 expression in T-cell acute lymphoblastic leukemia by acting as cofactors for GATA3. Mol Cell Biol 1998;18:6939–6950.
38 Mikkola HK, Klintman J, Yang H et al. Haematopoietic stem cells retain long-term repopulating activity and multipotency in the absence of stem-cell leukaemia SCL/tal-1 gene. Nature 2003;421:547–551.
39 Kunisato A, Chiba S, Saito T et al. Stem cell leukemia protein directs hematopoietic stem cell fate. Blood 2004;103:3336–3341.
40 Curtis DJ, McCormack MP. The molecular basis of Lmo2-induced T-cell acute lymphoblastic leukemia. Clin Cancer Res 2010;16:5618–5623.

See www.StemCells.com for supporting information available online.

Chemical Research in Toxicology

Article

pubs.acs.org/crt

In Vivo Drug Interactions of the Teratogen Thalidomide with Midazolam: Heterotropic Cooperativity of Human Cytochrome P450 in Humanized TK-NOG Mice

Hiroshi Yamazaki,*[,†] Hiroshi Suemizu,[‡] Norie Murayama,[†] Masahiro Utoh,[†] Norio Shibata,[§] Masato Nakamura,[‡] and F. Peter Guengerich*[,∥]

[†]Showa Pharmaceutical University, Machida, Tokyo 194-8543, Japan

[‡]Central Institute for Experimental Animals, Kawasaki-ku, Kawasaki 210-0821, Japan

[§]Graduate School of Engineering, Nagoya Institute of Technology, Showa-ku, Nagoya 466-8555, Japan

[∥]Department of Biochemistry, Vanderbilt University School of Medicine, Nashville, Tennessee 37232-0146, United States

ABSTRACT: In vivo drug interactions of the teratogen thalidomide with the model cytochrome P450 (P450) 3A substrate midazolam were investigated in mice with humanized livers. The clearance of midazolam (administered intravenously, 10 mg kg^{-1}) in chimeric mice was enhanced by orally co-administered thalidomide (100 mg kg^{-1}). A larger area under the curve of the major metabolite 1′-hydroxymidazolam (1.7-fold) was obtained with thalidomide because of the heterotropic cooperativity of human P450 3A enzymes. A larger area under the curve of the minor metabolite 4-hydroxymidazolam (3.5-fold) was seen with daily pretreatment with thalidomide for 3 days, presumably because of human P450 3A induction. These results demonstrate that livers of humanized mice mediate drug interactions of thalidomide and suggest interactions of therapeutic agents during therapies with thalidomide.

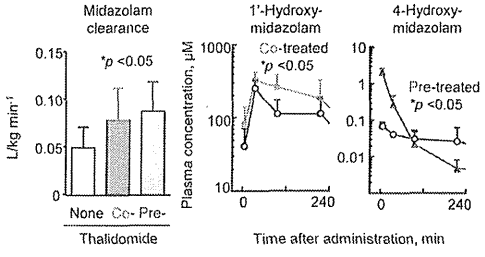

INTRODUCTION

Many drug interactions are caused by alterations in drug metabolism in the body, generally through enzyme inhibition or enzyme induction.[1] There is growing clinical interest in thalidomide because of its immunomodulatory and anti-angiogenic properties, despite its notorious teratogenicity in humans[2] (but its absence in rodents).[3] Little information about thalidomide with regard to its specific effects on human drug-metabolizing enzymes or drug interactions is available.[4] We previously reported, using in vitro systems, that midazolam metabolism or cyclosporine A clearance mediated by human liver microsomal cytochrome P450 3A4/5 may be enhanced by thalidomide in a dose-dependent manner, showing ligand cooperativity with P450 3A enzymes.[5]

We recently reported thalidomide 5-hydroxylation by human liver microsomal P450 3A4/5 and further aromatic ring oxidation leading to GSH conjugation, which may be relevant to the pharmacological and toxicological actions, in in vitro human situations[6] and in vivo chimeric mice with humanized liver cells.[7,8] In vivo ligand cooperativity with human P450 3A enzymes with humanized non-obese diabetes-severe combined immunodeficiency-interleukin-2 receptor γ chain-deficient mice (NOG mice) has not previously been reported. The purpose of this study was to investigate in vivo drug interactions of thalidomide with midazolam in NOG mice[9] containing human liver cells.[8] High midazolam clearance and a larger area-under-plasma-concentration time curve (AUC) of the metabolite 1′-hydroxymidazolam were obtained following co-administration of thalidomide, indicating that heterotropic cooperativity occurs in vivo. Thalidomide also has the potential for human P450 3A induction in chimeric mice with humanized liver, as judged by the rapid clearance of midazolam.

EXPERIMENTAL PROCEDURES

Chimeric Mice. Chemicals were from sources reported previously.[5,6,8] Male control TK-NOG and humanized TK-NOG mice (20−30 g body weight)[9] were used in this study. All mouse studies were performed in accordance with the guidelines of and were approved by the Animal Care Committee of the Japan Central Institute for Experimental Animals. All studies involving mouse tissue with transplanted human cells were approved by the Ethical and Biosafety Committee of the Japan Central Institute for Experimental Animals. Eight-week-old male TK-NOG mice received intraperitoneal injections of sodium ganciclovir (Denosine-IV, Mitsubishi Tanabe Pharma, Osaka, Japan) on days −7 and −5 prior to transplantation. One week after ganciclovir treatment, the degree of liver damage was examined by determining serum aspartate aminotransferase and alanine aminotransferase values (FUJI DRI-CHEM 7000, Fujifilm, Tokyo, Japan). For transplantation, 1×10^6 commercially available cryopreserved human hepatocytes [4-year-old, female (Lonza, Walkersville, MD)] were transplanted by intrasplenic injection as described previously.[9] Twelve weeks after transplantation, small amounts of blood were collected and human albumin concentrations were measured with the Human Albumin ELISA Quantitation Kit (Bethyl Laboratories, Montgomery, TX), according to the manufac-

Received: January 7, 2013
Published: February 18, 2013

turer's protocol. In these chimeric mice, >80% of liver cells were estimated to be replaced with human hepatocytes, as judged by measurements of human albumin concentrations in plasma.[9]

In Vivo Analysis. The U.S. Food and Drug Administration recommends the choice of midazolam for initial in vivo drug interaction studies for human P450 3A enzymes (http://www.fda.gov/). Blood samples were collected prior to and 5, 35, 95, 215, and 395 min after single oral doses of midazolam (10 mg kg^{-1}) administered to four animals. Racemic thalidomide [100 mg kg^{-1} (Wako Pure Chemicals, Osaka, Japan)] was orally administered 30 min before the midazolam treatment for the ligand cooperativity study. This dose was chosen because of the known pharmacokinetic profile[8] and the lack of apparent toxicity of thalidomide. In separated experiments, thalidomide (100 mg kg^{-1}) was administered to mice daily for 3 days for the induction study and followed by intravenous injection of midazolam on day 4. After treatment of the plasma samples with β-glucuronidase [from *Ampullaria*, 100000 units (Wako Pure Chemicals)], a 4-fold volume of CH_3OH containing 0.0625 μM caffeine (as an internal standard) was added. The aqueous supernatant was centrifuged at 2000*g* for 10 min at 4 °C and analyzed via LC–MS. The use of animals for this study was approved by the Ethics Committees of the Japan Central Institute for Experimental Animals and Showa Pharmaceutical University.

LC–MS/MS Analyses. LC–MS/MS analyses of midazolam and 1′- and 4-hydroxymidazolam were performed as described previously[5] with a slight modification. A Quattro micro API mass analyzer was used for the metabolite analysis (Waters, Tokyo, Japan). The instrument was operated in the electrospray positive ionization mode and was directly coupled to a Waters LC 2695 system with an octadecylsilane C_{18} column (Atlantis, 3 μm, 2.1 mm × 50 mm) and MassLynx NT4.1 software for data acquisition (Waters). To tune the mass spectrometer, the cone voltage was optimized to maximize the intensity of the precursor ions for midazolam at *m/z* 326.15. The collision energy was then adjusted to optimize the signal. Typical tuning conditions were as follows: electrospray capillary voltage, 3.0 kV; sample cone voltage, 36 V; and collision energy, 21.0 eV at a collision gas (Ar) pressure of 1.6×10^{-4} kPa. The gradient mobile phase consisted of 0.1% CH_3CO_2H and CH_3CN in 0.1% CH_3CO_2H (v/v): 0 to 95% CH_3CN (v/v) with 0.1% CH_3CO_2H (v/v) from 0 to 2.5 min, 95% CH_3CN (v/v) from 3 to 6.5 min, 95 to 0% CH_3CN with 0.1% CH_3CO_2H (v/v) from 6.5 to 7.0 min, and 0.1% CH_3CO_2H (v/v) from 7.0 to 13 min, all at a flow rate of 0.25 mL min^{-1}. Midazolam, its metabolites 1′- and 4-hydroxymidazolam, and the internal standard caffeine were quantified using the *m/z* 326 → 291 transition of midazolam, the *m/z* 342 → 325 transition of 1′- and 4-hydroxymidazolam, and the *m/z* 195 → 138 transition of caffeine, respectively.

Concentrations of midazolam and its metabolites were kinetically analyzed with WinNonlin (Pharsight, Sunnyvale, CA) and statically evaluated with a paired *t* test using Prism (GraphPad, San Diego, CA).

RESULTS

Because thalidomide was detected in mouse plasma 30 min after a single oral administration, as described previously,[7,8] intravenous midazolam administration (10 mg kg^{-1}) was conducted 30 min after thalidomide treatment (100 mg kg^{-1}) of male TK-NOG mice.[9] Thalidomide was previously administered orally to NOG mice daily for 3 days (100 mg kg^{-1}) followed by intravenous injection of midazolam on day 4. Midazolam and 1′- and 4-hydroxymidazolam were detected by LC–MS/MS analysis in mouse plasma samples prior to or 5–395 min after midazolam treatment. The time-dependent profiles of midazolam and its metabolites in chimeric mice with humanized liver are presented in Figure 1. In the control mice, midazolam was cleared from the plasma with a clearance (CL) value of 0.058 L kg^{-1} min^{-1} (Table 1). The main metabolite was 1′-hydroxymidazolam under these conditions. Cotreatment with thalidomide caused weak inhibition of midazolam

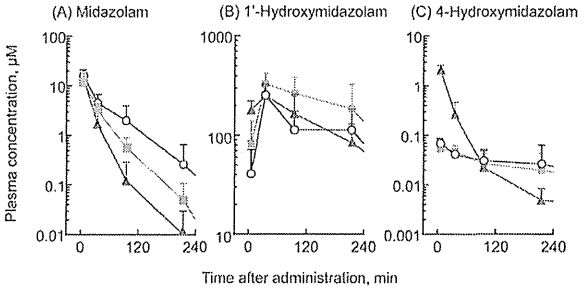

Figure 1. Plasma concentrations of midazolam (A), 1′-hydroxymidazolam (B), and 4-hydroxymidazolam (C) in chimeric NOG mice with humanized liver after single intravenous administrations (10 mg kg^{-1}) without (○) or with co-administration (■) or pretreatment (▲) with thalidomide (100 mg kg^{-1}). Thalidomide (100 mg kg^{-1}) was orally co-administered or administered daily for 3 days prior to intravenous midazolam treatment (10 mg kg^{-1}) in chimeric NOG mice with humanized liver. Results are expressed as means ± the standard deviation obtained with four mice in each set (*$p < 0.05$).

oxidation but did not affect CL or AUC significantly (Table 1). In contrast, midazolam clearance was enhanced (1.6-fold) by cotreatment with thalidomide (100 mg kg^{-1}) in chimeric mice with humanized liver (Figure 1A and Table 1). A significantly larger AUC of the major metabolite 1′-hydroxymidazolam [1.7-fold (Figure 1B and Table 1)] was observed when thalidomide was used, but not for the minor metabolite 4-hydroxymidazolam (Figure 1C), apparently because of the heterotropic cooperativity of human P450 3A enzymes in vivo. Pretreatment with thalidomide induced midazolam clearance in humanized NOG mice (Figure 1A and Table 1), but the small AUC of the minor metabolite 4-hydroxymidazolam was increased 3.5-fold (Figure 1C and Table 1) under these conditions. The pharmacokinetics of thalidomide and its metabolites in the humanized mice were described previously,[8] and rapid disappearance from the plasma to undetectable levels had been confirmed to occur within 24 h of oral treatment (100 mg kg^{-1}).

DISCUSSION

Limited information regarding thalidomide metabolism and drug interactions in vivo, especially in humans, is available. With renewed interest in thalidomide, subsequent work has confirmed that (aromatic ring) 4- and 5-hydroxylated metabolites of thalidomide are recovered in the urine of rabbits but not from rats.[10,11] Because humanized mice may generate more of the epoxide metabolite of thalidomide than control mice,[7,8] humanized liver might generally be a better model for possible drug interactions of thalidomide with midazolam. These results were similar when evaluated using in vitro human liver microsomes or recombinant P450 3A4/5 enzymes[5] and hepatic cell culture systems (data not shown) with regard to ligand cooperativity for the P450 3A enzymes.

Because human P450s 3A4 and 3A5 would be activated by heterotropic cooperativity of thalidomide, transformation of thalidomide to its 1′-hydroxy metabolite was enhanced by co-administration in chimeric mice with humanized liver (Figure 1 and Table 1). When the total mass balance was considered, an increase in the AUC of 1′-hydroxymidazolam after co-administration with thalidomide would be recognized, probably because of the slower elimination of 1′-hydroxymidazolam than the parent compound. In our preliminary experiments using

dx.doi.org/10.1021/tx400008g | *Chem. Res. Toxicol.* 2013, 26, 486–489

Table 1. Pharmacokinetic Parameters for Midazolam and Its Metabolites in Control NOG Mice and Chimeric Mice with Humanized Liver after a Single Intravenous Administration (10 mg kg^{-1}), with or without Co-Administration or Pretreatment with Thalidomide (100 mg kg^{-1})[a]

	CL (L kg^{-1} min^{-1})	$AUC_{0-\infty}$ (μM min)		
	midazolam	midazolam	1′-hydroxymidazolam	4-hydroxymidazolam
	(1) Control NOG Mice			
midazolam alone	0.058 ± 0.005	536 ± 46	29700 ± 6800	72.7 ± 5.3
co-administered with thalidomide	0.051 ± 0.010	616 ± 130	14300 ± 2500	51.2 ± 15.3
	(2) Mice with Humanized Liver			
midazolam alone	0.049 ± 0.022	759 ± 431	42600 ± 15000	15.0 ± 8.0
co-administered with thalidomide	0.078 ± 0.034*	459 ± 202	72300 ± 31500*	14.0 ± 5.9
pretreated with thalidomide	0.087 ± 0.031*	383 ± 120	46800 ± 18000	52.1 ± 16.7*

[a]Thalidomide (100 mg kg^{-1}) was orally co-administered or administered daily for 3 days prior to intravenous midazolam treatment (10 mg kg^{-1}) in control NOG mice and chimeric NOG mice with humanized liver. Data are means ± the standard deviation with four mice in each set (*$p < 0.05$).

human hepatocyte systems, thalidomide, but not the primary human metabolite 5-hydroxythalidomide, was a good activator for P450 3A enzymes responsible for midazolam 1′-hydroxylation. With regard to ligand cooperativity, unmetabolized thalidomide was responsible for activation of human P450 3A enzymes. Because the primary metabolites of thalidomide might not be involved the P450 3A activation, the secondary reactive epoxide metabolite(s) derived from 5-hydroxythalidomide should also not be the human P450 3A activator. This hypothesis was consistent with the high plasma concentrations of 1′-hydroxymidazolam in chimeric mice at the earliest time after the administration of thalidomide when parent compound concentrations would be sufficient. On the other hand, human P450 3A4 in chimeric livers might be more highly induced than P450 3A5 in the case of pretreatment with thalidomide, resulting in the AUC of 4-hydroxymetabolite being predominantly larger. Rapid elimination of 4-hydroxymidazolam might be ascribed to the possible secondary metabolism of the primary metabolite mediated by induced human P450 3A4. Regardless, differences in species susceptibility may result from differences in the in vivo disposition and biotransformation of thalidomide by drug-metabolizing enzymes, resulting in drug interactions.

In this study, we analyzed the effects of thalidomide on midazolam metabolism in vivo using humanized NOG mice in which the liver was replaced with transplanted human liver cells. Thus, these results address the issue of drug interactions of thalidomide in vivo (Figure 1). The possible metabolism of thalidomide by intestinal mouse P450s has not yet been considered in a setting in which the drug is administered orally to chimeric mice with humanized liver.

In conclusion, this study demonstrates that human liver cells expressed in chimeric NOG mice effectively mediate enhancement of midazolam metabolism by thalidomide in vivo via ligand cooperativity. The possibilities of reactive metabolite formation and of drug interactions during thalidomide therapy in humans should be evaluated further.

AUTHOR INFORMATION

Corresponding Author

*H.Y.: Showa Pharmaceutical University, 3-3165 Higashi-tamagawa Gakuen, Machida, Tokyo 194-8543, Japan; telephone, +81-42-721-1406; fax, +81-42-721-1406; e-mail, hyamazak@ac.shoyaku.ac.jp. F.P.G.: Department of Biochemistry, Vanderbilt University School of Medicine, Nashville, TN 37232-0146; telephone, (615) 322-2261; fax, (615) 322-4349; e-mail, f.guengerich@vanderbilt.edu.

Author Contributions

H.Y. and H.S. contributed equally to this work.

Funding

This work was supported in part by the Ministry of Education, Culture, Sports, Science, and Technology of Japan (H.Y.) and U.S. Public Health Service Grant R37 CA090426 (F.P.G.).

Notes

The authors declare no competing financial interest.

ACKNOWLEDGMENTS

We thank Drs. Shika Inoue, Miyuki Kuronuma, and Makiko Shimizu for their technical assistance.

ABBREVIATIONS

AUC, area-under-plasma-concentration time curve; CL, clearance; NOG mice, non-obese diabetes-severe combined immunodeficiency-interleukin-2 receptor γ chain-deficient mice

REFERENCES

(1) Rendic, S., and Guengerich, F. P. (2010) Update information on drug metabolism systems—2009, part II: Summary of information on the effects of diseases and environmental factors on human cytochrome P450 (CYP) enzymes and transporters. *Curr. Drug Metab. 11*, 4–84.

(2) Calabrese, L., and Resztak, K. (1998) Thalidomide revisited: Pharmacology and clinical applications. *Expert Opin. Invest. Drugs 7*, 2043–2060.

(3) Kim, J. H., and Scialli, A. R. (2011) Thalidomide: The tragedy of birth defects and the effective treatment of disease. *Toxicol. Sci. 122*, 1–6.

(4) Trapnell, C. B., Donahue, S. R., Collins, J. M., Flockhart, D. A., Thacker, D., and Abernethy, D. R. (1998) Thalidomide does not alter the pharmacokinetics of ethinyl estradiol and norethindrone. *Clin. Pharmacol. Ther. 64*, 597–602.

(5) Okada, Y., Murayama, N., Yanagida, C., Shimizu, M., Guengerich, F. P., and Yamazaki, H. (2009) Drug interactions of thalidomide with midazolam and cyclosporine A: Heterotropic cooperativity of human cytochrome P450 3A5. *Drug Metab. Dispos. 37*, 18–23.

(6) Chowdhury, G., Murayama, N., Okada, Y., Uno, Y., Shimizu, M., Shibata, N., Guengerich, F. P., and Yamazaki, H. (2010) Human liver microsomal cytochrome P450 3A enzymes involved in thalidomide 5-hydroxylation and formation of a glutathione conjugate. *Chem. Res. Toxicol. 23*, 1018–1024.

(7) Yamazaki, H., Suemizu, H., Igaya, S., Shimizu, M., Shibata, M., Nakamura, M., Chowdhury, G., and Guengerich, F. P. (2011) *In vivo* formation of a glutathione conjugate derived from thalidomide in humanized uPA-NOG mice. *Chem. Res. Toxicol. 24*, 287–289.

(8) Yamazaki, H., Suemizu, H., Shimizu, M., Igaya, S., Shibata, N., Nakamura, N., Chowdhury, G., and Guengerich, F. P. (2012) *In vivo*

formation of dihydroxylated and glutathione conjugate metabolites derived from thalidomide and 5-hydroxythalidomide in humanized TK-NOG mice. *Chem. Res. Toxicol. 25*, 274−276.

(9) Hasegawa, M., Kawai, K., Mitsui, T., Taniguchi, K., Monnai, M., Wakui, M., Ito, M., Suematsu, M., Peltz, G., Nakamura, M., and Suemizu, H. (2011) The reconstituted 'humanized liver' in TK-NOG mice is mature and functional. *Biochem. Biophys. Res. Commun. 405*, 405−410.

(10) Eriksson, T., Bjorkman, S., Roth, B., Bjork, H., and Hoglund, P. (1998) Hydroxylated metabolites of thalidomide: Formation *in-vitro* and *in-vivo* in man. *J. Pharm. Pharmacol. 50*, 1409−1416.

(11) Schumacher, H., Smith, R. L., and Williams, R. T. (1965) The metabolism of thalidomide: The fate of thalidomide and some of its hydrolysis products in various species. *Br. J. Pharmacol. Chemother. 25*, 338−351.

Regulatory Toxicology and Pharmacology 65 (2013) 316–324

Contents lists available at SciVerse ScienceDirect

Regulatory Toxicology and Pharmacology

journal homepage: www.elsevier.com/locate/yrtph

Plasma concentrations of melengestrol acetate in humans extrapolated from the pharmacokinetics established in *in vivo* experiments with rats and chimeric mice with humanized liver and physiologically based pharmacokinetic modeling

Ai Tsukada [a], Hiroshi Suemizu [b], Norie Murayama [a], Ryohji Takano [a,c], Makiko Shimizu [a], Masato Nakamura [b], Hiroshi Yamazaki [a,*]

[a] *Laboratory of Drug Metabolism and Pharmacokinetics, Showa Pharmaceutical University, Machida, Tokyo 194-8543, Japan*
[b] *Central Institute for Experimental Animals, Kawasaki-ku, Kawasaki 210-0821, Japan*
[c] *Fujitsu Kyusyu Systems, Fukuoka 814-8589, Japan*

ARTICLE INFO

Article history:
Received 3 September 2012
Available online 5 February 2013

Keywords:
Physiologically based biokinetic model
Transplanted human liver
No-observed-adverse-effect level
Simulation
Allometric scaling

ABSTRACT

Some synthetic chemicals are suspected to be responsible for adverse effects on endocrine function. Sex hormones administered to farm animals are of particular interest because of their regulatory role in developmental processes. To predict concentrations in humans of the synthetic growth promoter melengestrol acetate (17α-acetoxy-6-methyl-16-methylenepregna-4,6-diene-3,20-dione), a forward dosimetry approach was carried out using data from no-observed-adverse-effect-level doses orally administered to mice or rats and from *in vitro* human and rodent experiments. Human liver microsomes preferentially mediated 2-hydroxylation of melengestrol acetate, but rodent livers produced additional unidentified hydroxymetabolites. Adjusted animal biomonitoring equivalents for melengestrol acetate from mouse and rat studies were scaled to human biomonitoring equivalents using known species allometric scaling factors and human metabolic data with a simple physiologically based pharmacokinetic (PBPK) model. Melengestrol acetate elimination in humans was estimated to be slow compared with elimination in rodents. The disposition of melengestrol acetate in humans was evaluated using chimeric TK-NOG mice with humanized liver. The results suggest the usefulness of simplified PBPK modeling combined with *in vitro* and *in vivo* experiments and literature resources as well as a future interest in estimating by a full PBPK modeling using another bottom up system. This model may also be useful for risk evaluation and for simulating plasma concentrations resulting from exposure to low doses of melengestrol acetate and related compounds.

1. Introduction

It is of global interest to develop simple, advanced, and accurate risk assessment systems to support the interpretation of data from human biomonitoring studies (Wild, 2005). Using dose estimates instead of external or applied doses can improve the characterization of dose–response relationships and the subsequent characterization of potential health risks. This improvement results from the direct relationship between internal dosimetry (shown in Fig. 1) and the biological response. Pharmacokinetic and/or toxicokinetic parameters for a variety of chemicals have been determined in animal toxicology studies, despite the species differences of drug-metabolizing enzymes (Clewell et al., 2004). Such data for humans is often very limited. Human health risk assessments use the dose–response relationship to characterize and quantify potential health risks. When relevant and reliable estimates of the internal dose of a compound or a key metabolite are available, the results of toxicology studies can often be better understood and evaluated in terms of the internal dose. It has been attempted to collect extensive information regarding specific physiologically based pharmacokinetic (PBPK) models found in the literature for predicting concentrations in various biological fluids following multiple dose exposures (Edwards and Preston, 2008; McLanahan et al., 2012). However, although simple, inexpensive, and reliable methods are needed for accurately evaluating the toxic risk (McLanahan et al., 2012), very few such methods have been established. For example, a nine-compartment PBPK model for acrylonitrile and its primary metabolite in humans has been reported (Sweeney et al., 2003); however, we proposed a simple and reliable PBPK model capable

* Corresponding author. Address: Laboratory of Drug Metabolism and Pharmacokinetics, Showa Pharmaceutical University, 3-3165 Higashi-tamagawa Gakuen, Machida, Tokyo 194-8543, Japan. Fax: +81 42 721 1406.
E-mail address: hyamazak@ac.shoyaku.ac.jp (H. Yamazaki).

0273-2300/$ - see front matter © 2013 Elsevier Inc. All rights reserved.
http://dx.doi.org/10.1016/j.yrtph.2013.01.008

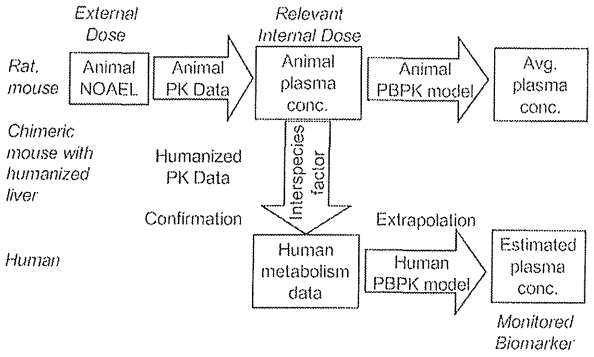

Fig. 1. Approach for calculating blood-based biomonitoring equivalents for melengestrol acetate. NOAEL, no-observed-adverse-effect level; PK, pharmacokinetics; PBPK, physiologically based pharmacokinetic.

of both forward and reverse dosimetry approaches (Takano et al., 2010).

As one of candidate compounds with the concern of long-term intaking risk, the synthetic progesterone melengestrol acetate (17α-acetoxy-6-methyl-16-methylenepregna-4,6-diene-3,20-dione is of high potency as a progestin (Perry et al., 2005) and is used as a growth promoter for farm animals in several meat-exporting countries (Lauderdale et al., 1977; Perry et al., 2005). This has led to international disputes about the safety of meat originating from treated animals (Patterson et al., 1989). Although many studies have explored its safety with respect to both animals and meat consumers (Stephany, 2010), little is known about the fate of melengestrol acetate in humans (Cooper et al., 1967; Elce et al., 1967) or its potential endocrine-disrupting activity (Schiffer et al., 2001). Melengestrol acetate has been shown to be biotransformed to mono- and dihydroxymelengestrol acetate (including 2-hydroxylated and 6-hydroxymethylated metabolites) in rodents, but the hormonal or biological potential of these chemical species in humans has not been fully elucidated (Cooper et al., 1967; Elce et al., 1967; Metzler and Pfeiffer, 2001) under the concern of long-term risk of melengestrol acetate intake in no-observed-adverse-effect level. Recently developed TK-NOG mice transplanted with human liver cells can survive without ongoing drug treatment (Hasegawa et al., 2011; Yamazaki et al., 2012). Because such survival was not achieved in previous liver reconstruction models, it is now possible to evaluate the estimates obtained from simplified human PBPK modeling by comparing them with *in vivo* experimental results from mice with humanized liver.

The purpose of the present study was to predict melengestrol acetate plasma concentrations in humans by a forward dosimetry analysis (Fig. 1) using data from chemical doses administered to animals and from *in vitro* experiments with liver microsomes from humans and animals. The adjusted animal biomonitoring equivalents after orally administered doses in rat and mouse studies were scaled to human biomonitoring equivalents using known species allometric scaling factors and human metabolic data with a simple PBPK model. According to the present PBPK analysis, the synthetic progesterone melengestrol acetate is cleared slowly in humans compared with clearance in rodents.

2. Materials and methods

2.1. Chemicals, animals, and enzyme preparations

Male 6-week-old Sprague–Dawley rats (Charles River Laboratory Japan, Tokyo, Japan) and control TK-NOG and humanized TK-NOG mice (~20–30 g body weight) (Hasegawa et al., 2011) were used in this study. In the chimeric mice, more than 80% of liver cells were estimated to have been replaced with human hepatocytes, as judged by measurements of human albumin concentrations in plasma (Hasegawa et al., 2011; Yamazaki et al., 2012). Plasma samples were collected 0.5, 1, 2, 4, 7, and 24 h after single oral doses of melengestrol acetate (3.0–100 mg/kg, Wako Pure Chemicals, Tokyo, Japan). For rats, 3.0 mg/kg of melengestrol acetate was reported to have no observed adverse effect (Joint FAO/WHO Expert Committee, 2009). The use of animals for this study was approved by the Ethics Committees of the Japan Central Institute for Experimental Animals and Showa Pharmaceutical University. Liver microsomes from 7-week-old male rats and mice were prepared as described previously (Yamazaki et al., 2006; Yamazaki et al., 2011). Protein concentrations were estimated by using a bicinchoninic acid protein assay kit (Pierce, Rockford, IL, USA). Microsomes from pooled human livers (H150) and recombinant P450 enzymes were obtained from BD Biosciences (Woburn, MA, USA). Other reagents used in this study were obtained from sources described previously or were of the highest quality commercially available (Murayama et al., 2009; Yamazaki et al., 2006).

2.2. In vitro and in vivo metabolic studies of melengestrol acetate

Elimination rates of melengestrol acetate in liver microsomes from rats, mice, and humans were measured by a liquid chromatography (LC) system. Briefly, a typical incubation mixture consisted of 100 mM potassium phosphate buffer (pH 7.4), an NADPH-generating system, melengestrol acetate (10 μM), and liver microsomes (0.25 mg protein/mL) or recombinant P450 enzymes (0.040 μM) in a final volume of 0.50 mL. Incubations were carried out at 37 °C for 15 min. Reactions were terminated by adding 3.0 mL of ethyl acetate. After treatment of the plasma samples (20 μL) from individual rats and mice with methanol (120 μL) for deproteinization, melengestrol acetate and its metabolites were exacted with ethyl acetate (300 μL). After vortex mixing, the tubes were centrifuged at 1000g for 10 min. The organic phase was transferred to a clean tube and evaporated to dryness at 40 °C under a gentle nitrogen stream. The residue was dissolved in 0.12–0.20 mL of mobile phase. Melengestrol acetate and its metabolites in the incubation mixtures and plasma samples were determined by LC. The LC system consisted of a pump and multi-wavelength UV detector (Shimadzu, Kyoto, Japan) using an analytical C_{18} reversed-phase column (5 μm, 4.6 × 250 mm, Mightysil RP-18 GP, Kanto Chemicals, Tokyo, Japan). The mobile phase was 55% acetonitrile in 1.0% CH_3CO_2H, at a flow rate of 1.5 mL/min. The UV detector was set at a wavelength of 280 nm unless otherwise specified. The LC apparatus was operated at room temperature. Metabolites were quantified on the basis of the standard curve peak area at UV 280 nm of melengestrol acetate.

Statistical analysis of the plasma concentrations of melengestrol acetate and its metabolites in rats and mice and control and humanized mice were done using two-way analysis of variance (ANOVA) with Bonferroni post tests (Prism, GraphPad Software, La Jolla, CA, USA). Area under the curve (AUC) values were derived from plots of melengestrol and its metabolites versus time and were calculated using the trapezoidal rule with the program WinNonlin (Pharsight, Sunnyvale, CA, USA).

2.3. LC/tandem mass spectrometry assay

A Quattro micro API mass analyzer was used for metabolite analysis (Waters, Tokyo, Japan) using an LC/tandem mass spectrometry (LC-MS/MS) system. The instrument was operated in electrospray positive ionization mode and was directly coupled to the LC 2695 system (Waters) with a C_{18} column (Xbrige, 3.5 μm, 2.1 × 150 mm), and MassLynx NT4.1 software was used

for data acquisition (Waters). To tune the mass spectrometer, a solution of melengestrol acetate (10 ppm in a mobile phase) was infused into the ion source, and the cone voltage was optimized to maximize the intensity of the precursor ions for melengestrol acetate (*m/z* 397.5). The collision energy was then adjusted to optimize the signal for one of the most abundant melengestrol product ions (*m/z* 337). Typical tuning conditions were as follows: electrospray capillary voltage, 3.0 kV; sample cone voltage, 30 V; and collision energy, 20 eV at a collision gas pressure 1.6×10^{-4} kPa argon.

MS analyses were performed for melengestrol acetate and its hydroxylated metabolites. The mass spectrometer was tuned using melengestrol acetate. LC conditions were as follows: buffer A contained 1.0% CH_3CO_2H in CH_3CN and buffer B contained 1.0% CH_3CO_2H in H_2O (v/v). The following gradient program was used at a flow rate of 0.20 mL min^{-1}: 0–25 min, linear gradient from 55% A to 80% A (v/v); 25–30 min, hold at 80% A; 30–32 min, linear gradient to 55% A; 32–40 min, hold at 55% A. The temperature of the column was maintained at 40 °C. Samples (10 μL) were injected with an auto-sampler. MS analyses were performed for melengestrol acetate and its hydroxylated metabolites. Melengestrol acetate and 2-hydroxymelengestrol acetate were analyzed using the *m/z* 397.5 → 337.5 transition of melengestrol acetate and the *m/z* 353 → 125 transition of 2-hydroxymelengestrol acetate.

2.4. Estimation of melengestrol acetate concentrations using a PBPK model with suitable parameters

A simplified PBPK model (Fig. 2) was set up as described previously (Gargas et al., 1995; Kato et al., 2008; Takano et al., 2010; Yamazaki et al., 2010). The model basically consists of a chemical receptor compartment, a metabolizing compartment, and a central compartment (Gargas et al., 1995; Kato et al., 2008; Takano et al., 2010; Yamazaki et al., 2010) (Fig. 2). The values of the physicochemical properties of melengestrol acetate and 2-hydroxymelengestrol acetate are shown in Table 1. Values of the plasma unbound fraction ($f_{u,p}$) and the octanol–water partition coefficient (logP) were obtained by *in silico* estimation using SimCYP and ChemDrawBioUltra software (Emoto et al., 2009); the liver–plasma concentration ratio ($K_{p,h}$) and the blood to plasma concentration ratio (R_b) were estimated from $f_{u,p}$ and logP (Appendix A). Values of $f_{u,mic}$ (5.0%) and $f_{u,p}$ (30%) of melenegestrol acetate were experimentally confirmed by LC measurements of ultrafiltrates from 1.0 and 40 mg/mL of bovine serum albumin solution in 50 mM Tris–HCl buffer (pH 7.4). Hydrophobicity of melengestrol acetate was confirmed by the PubChem Compound (XLogP3-AA value of 3.1).

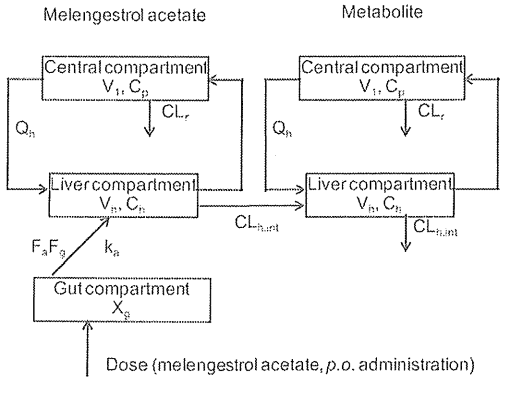

Fig. 2. PBPK model established in this study for rats, mice and humans. X_g, melengestrol acetate amount in the gut; C_h, hepatic substance concentration; and C_b blood substance concentration. For other definitions, see Table 2.

Parameters that represent physiological properties such as hepatic volumes and blood flow rates in rats, mice, and humans were taken from the literature (Gargas et al., 1995; Kato et al., 2008).

Experimental plasma concentrations of melengestrol acetate and its metabolites were analyzed using WinNonlin software (Professional version 5.2.1) with a one-compartment model and yielded primary absorption rate constant (k_a), and elimination constant (k_{el}) values as pharmacokinetic parameters. Values of the total clearance (CL_{tot}), hepatic clearance (CL_h), hepatic intrinsic clearance ($CL_{h,int}$), and the volume of the systemic circulation (V_1) were also calculated (Appendix A). Subsequently, final parameter values for the rat and mouse PBPK models were calculated using the initial values mentioned above by the user model in WinNonlin; these parameters are shown in Tables 1 and 2. Consequently, the following system of differential equations were solved to conduct the modeling for melengestrol acetate:

$$\frac{dX_g(t)}{dt} = -k_a \cdot X_g(t) \quad \text{where at } t = 0, X_g(0) = \text{dose}$$

$$V_h \frac{dC_h}{dt} = Q_h \cdot C_b - \frac{Q_h \cdot C_h \cdot R_b}{K_{p,h}} + k_a \cdot X_g - CL_{h,int} \cdot \frac{C_h}{K_{p,h}} \cdot f_{u,p}$$

$$V_1 \frac{dC_b}{dt} = -Q_h \cdot C_b + \frac{Q_h \cdot C_h \cdot R_b}{K_{p,h}} - CL_r \cdot C_b$$

where X_g is the melengestrol acetate amount in the gut, C_h is the hepatic substance concentration, and C_b is the blood substance concentration.

For the metabolite:

$$V_1 \frac{dC_b}{dt} = -Q_h \cdot C_b + \frac{Q_h \cdot C_h \cdot R_b}{K_{p,h}} - CL_r \cdot C_b$$

$$V_h \frac{dC_h}{dt} = Q_h \cdot C_b - \frac{Q_h \cdot C_h \cdot R_b}{K_{p,h}} - CL_{h,int} \cdot \frac{C_h}{K_{p,h}} \cdot f_{u,p} + CL_{h,int,metabolite} \cdot \frac{C_{h,metabolite}}{K_{p,h,metabolite} \cdot f_{u,p,metabolite}}$$

To define a simplified PBPK model for melengestrol acetate and its metabolite in humans based on the rat or mouse PBPK model, we used relevant liver microsomes and physiological parameters (CL_r, k_a, and V_1) derived from the literature and applied the systems approach to fit them into the traditional parallelogram for risk assessment (Edwards and Preston, 2008). The values of CL_h, k_a, and V_1 in the human PBPK model were estimated using a scale-up strategy from rats and mice to humans as follows. The human hepatic (or renal) clearance CL_{human} was estimated using Eq. (1), where $BW_{rodent} = 0.25$ (rat) or 0.025 (mouse) kg and $BW_{human} = 70$ kg:

$$CL_{h,human} = \frac{CL_{h,rodent}}{BW_{rodent}^{(\frac{2}{3})}} \cdot BW_{human}^{(\frac{2}{3})} \quad (1)$$

The human absorption rate constant (k_a) was estimated as (Amidon et al., 1988):

$$k_{a,human} = 0.774 \cdot k_{a,rodent} \quad (2)$$

The human systemic circulation volume ($V_{1,human}$) was estimated from Eqs. (3),4, where $V_{h,human}$, $V_{b,rodent}$, and $V_{b,human}$ were 1.50 L, 0.0160 (rat) and 0.00160 (mouse) L, and 4.90 L, respectively:

$$V_{d,human} = V_{b,human} + (V_{d,rodent} - V_{b,rodent}) \cdot \frac{R_{b,rodent}}{f_{u,p,rodent}} \cdot \frac{f_{u,p,human}}{R_{b,human}} \quad (3)$$

$$V_{1,human} = V_{d,human} - V_{h,human} \cdot \frac{K_{p,h}}{R_b} \cdot F_h \quad (4)$$

Table 1
Chemical properties of melengestrol acetate and 2-hydroxymelengestrol acetate (M3).

Parameter	Symbol	Melengestrol acetate	2-Hydroxy-melengestrol acetate
Molecular weight	MW	397	413
Octanol–water partition coefficient	logP	4.02	3.16
Plasma unbound fraction	$f_{u,p}$	0.0450	0.103
Fraction unbound in microsomes	$f_{u,mic}$	0.299	0.545
Ratio of the blood to plasma concentration	R_b	0.765	0.834
Liver–plasma concentration ratio	$K_{p,h}$	2.96	2.79

2-Hydroxymelengestrol acetate was identified in Fig. 3 in this study.

Table 2
Physiological and experimentally determined parameters for melengestrol acetate disposition in rats, mice, and humans.

Parameter	Symbols (unit)	Rat	Mouse	Human, from rat	Human, from mouse
Body weight	BW (kg)	0.25	0.025	70	70
Liver weight	Liver weight (g)	10	1.5	1500	1500
Hepatic blood flow rate of systemic circulation to the tissue compartment	Q_h (L/h)	0.853	0.160	96.6	96.6
Volume of systemic circulation	V_1 (L)	0.00850	0.000850	1.50	1.50
Volume of blood	V_b (L)	0.0160	0.00160	4.90	4.90
Ratio of the blood to plasma concentration, substrate	R_{b_MGA}	0.765	0.765	0.765	0.765
Renal clearance, for MGA	CL_{r_MGA} (L/h)	0	0	0	0
Hepatic intrinsic clearance, for MGA	CL_{h,int_MGA} (L/h)	284	99.7	81000	140000
Volume of systemic circulation, for MGA	V_{1_MGA} (L)	2.24	0.144	628	404
Absorption rate constant, for MGA	k_{a_MGA} (1/h)	2.23	2.50	1.66	1.86
Fraction absorbed × intestinal availability	F_aF_g	1	1	1	1
Metabolic ratio to M3		0.35	0.37	0.76	0.76
Ratio of the blood to plasma concentration, for metabolite	R_{b_M3}	0.830	0.830	0.830	0.830
Renal clearance, for metabolite	CL_{r_M3} (L/h)	0	0	0	0
Hepatic intrinsic clearance, for metabolite	CL_{h,int_M3} (L/h)	18.4	2.98	5250	4170
Volume of systemic circulation, for metabolite	V_{1_M3} (L)	5.38	1.13	1510	3170

Some other parameters are shown in Tables 1 and 3. MGA, melengestrol acetate; M3, 2-hydroxymelengestrol acetate, as identified in Fig. 3 in this study.

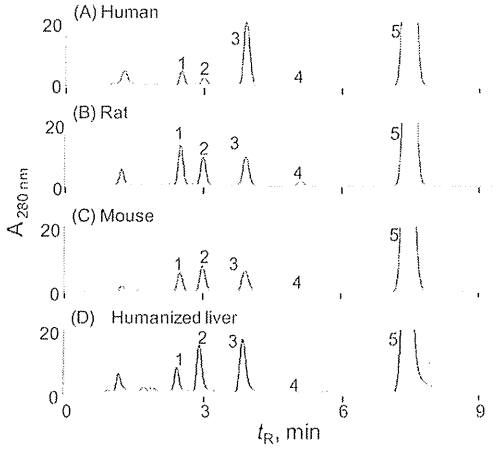

Fig. 3. Representative chromatograms for *in vitro* metabolites of melengestrol acetate produced by liver microsomes from pooled human livers (A), rats (B), mice (C), and humanized livers transplanted into chimeric mice (D). Melengestrol acetate (10 μM) was incubated with liver microsomes (0.25 mg/mL) at 37 °C for 15 min. Extracted metabolites were separated with a reverse-phase LC. Peak 1, unidentified dihydroxymelengestrol acetate (M1, suggested by LC-MS/MS analysis by addition of two oxygen atoms, plus 32 *m/z*); peak 2, unidentified monohydroxymelengestrol acetate (M2, by addition of one oxygen atom, plus 16 *m/z*); peak 3, 2-hydroxymelengestrol acetate (M3, see Fig. 4); peak 4, unidentified monohydroxymelengestrol acetate (M4, by addition of one oxygen atom, plus 16 *m/z*); and peak 5, melengestrol acetate. The metabolites M1–M4 were quantified on the basis of the standard curve peak area at UV 280 nm of melengestrol acetate (see Table 3). M1, M2, and M4 were estimated to be 2,15-dihydroxymelengestrol acetate, 15-hydroxymelengestrol acetate, and 6-hydroxymethyl-melengestrol acetate, respectively, according to information found in the literature.

where physicochemical parameters such as $K_{p,h}$, R_b, and $f_{u,p}$ (shown in Appendix A) were assumed to be the same for rats and humans.

The *in vivo* hepatic intrinsic clearance ($CL_{h,int}$) of melengestrol acetate in humans was estimated by multiplying the calculated initial parameters for *in vitro* hepatic intrinsic clearance values in humans by the ratio of *in vivo* to *in vitro* hepatic intrinsic clearance in rats or mice, as mentioned above for modeling in rats and mice. Then, the final parameters for the human PBPK model were calculated using these initial values by the user model in WinNonlin; these parameters are shown in Table 2. As was done for the rat and mouse models, systems of differential equations were solved to determine the concentrations in each compartment in humans.

3. Results

3.1. Metabolism of melengestrol acetate

The *in vitro* metabolism of melengestrol acetate was investigated using liver microsomes from pooled human livers, rats, mice, and chimeric mice with humanized liver. Typical chromatograms are shown in Fig. 3 after the incubation of melengestrol acetate (10 μM) with liver microsomes; four metabolite peaks (designated as peaks 1–4 in Fig. 3) and peak 5 (assigned to melengestrol acetate) were observed. The four metabolites were present in different proportions in all reaction mixtures. The rates of metabolite formation and melengestrol acetate elimination were determined (Table 3). Liver microsomes from rats and mice formed M1, M2, and M3 at roughly similar rates, but human liver microsomes preferentially produced M3. Liver microsomes prepared from transplanted human hepatocytes in chimeric mice mainly catalyzed M3 formation, followed by M2 production. Based on the melengestrol acetate elimination rates in these liver microsomes, hepatic intrinsic clearance ($CL_{h,int,in\ vitro}$) rates were calculated (Table 3) from the elimination rates, substrate concentration, and unbound fractions ($f_{u,mic}$) of 0.299 determined by SimCYP software for use in the PBPK models. Estimated clearance values ($CL_{h,int,in\ vitro}$) were extrapo-

Table 3
Rates of metabolite formation, melengestrol acetate elimination, and hepatic intrinsic clearance ($CL_{h,int,in\ vitro}$) determined using liver microsomes from pooled human livers, rats, mice, and chimeric mice with humanized liver.

Enzyme source	Metabolite formation (pmol/min/mg protein)				Melengestrol acetate elimination (pmol/min/mg protein)	$CL_{h,int,in\ vitro}$ (L/h)
	M1	M2	M3[a]	M4		
Human	79	56	449	7	855	1030
Rat	121	121	148	27	451	3.61
Mouse	100	210	187	8	612	0.736
Chimeric mouse	111	211	358	8	755	0.908[b]/910[c]

Melengestrol acetate (10 μM) was incubated with liver microsomes (0.25 mg/mL) at 37 °C for 15 min. Extracted metabolites were separated with a reverse-phase LC. Estimated clearance values ($CL_{h,int,in\ vitro}$) were extrapolated using the fraction unbound in liver microsomes and following values: 40 mg liver microsomal protein per 1 g liver and 10 g liver weight per 0.25 kg of rat BW, 1.5 g liver weight per 0.025 kg of mouse BW or 1.5 kg liver weight per 70 kg of human BW.

[a] M3, 2-hydroxymelengestrol acetate, as identified in Fig. 3 in this study. Two $CL_{h,int,in\ vitro}$ values are shown accoding to mouse[b] or human[c] liver sizes.

Table 4
Rates of metabolite formation and melengestrol acetate elimination determined using recombinant human P450 enzymes.

P450 enzyme	Metabolite formation (nmol/min/nmol P450)				Melengestrol acetate elimination (nmol/min/nmol P450)
	M1	M2	M3[a]	M4	
1A2	0.035	0.011	0.010	0.046	0.497
2C9	0.124	0.012	0.022	0.044	0.387
2C19	0.106	0.012	0.013	0.045	0.555
2D6	0.052	0.010	0.074	0.046	0.498
2E1	0.020	0.014	0.006	0.046	0.478
3A4	0.919	0.578	8.83	0.054	16.2

Melengestrol acetate (10 μM) was incubated with recombinant human P450 (0.04 nmol/mL) at 37 °C for 15 min. Extracted metabolites were separated with a reverse-phase LC.

[a] M3, 2-hydroxymelengestrol acetate identified in Fig. 3 in this study.

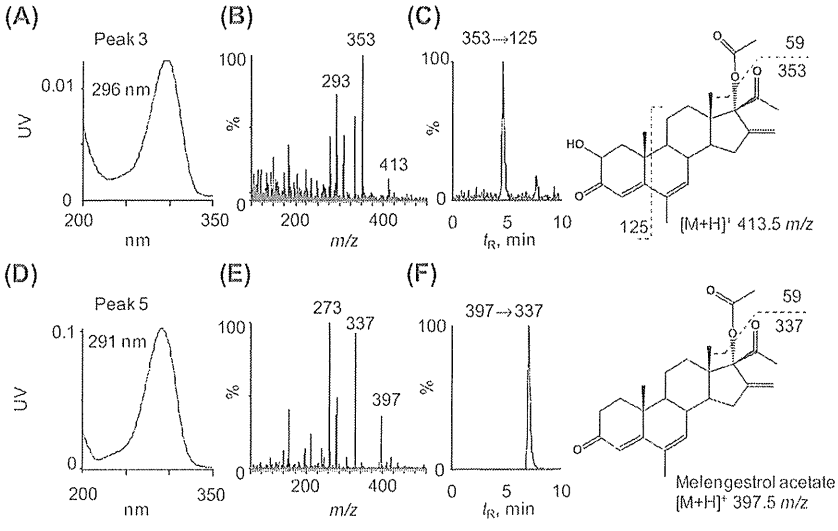

Fig. 4. UV spectra (A, D), LC-MS spectra (B,E), and LC-MS/MS chromatograms (C, F) of primary metabolite 2-hydroxymelengestrol acetate (A–C) and substrate melengestrol acetate (D–F) in human liver microsomes. An extracted ion chromatogram of the product ion with *m/z* 353 → 125 of 2-hydroxymelengestrol acetate (C) is shown for incubation mixtures with human liver microsomes and melengestrol acetate.

lated using the following values: 40 mg liver microsomal protein per 1 g liver and 10 g liver weight per 0.25 kg of rat BW, 1.5 g liver weight per 0.025 kg of mouse BW or 1.5 kg liver weight per 70 kg of human BW. For example, human $CL_{h,int,in\ vitro}$ value of 1030 L/h (Table 3) was obtained by following calculation: 855 (pmol/min/mg protein)/ ($10 \times 10^{-6} \times 0.299$ (μmol/L) × 60 min/h × 40 (mg protein/g liver) × 1500 (g liver). Among the recombinantly expressed human P450 isoforms tested, P450 3A4 preferentially catalyzed the transformation of melengestrol acetate to M3, accounting for approximately half of the eliminated melengestrol acetate (Table 4).

The metabolite seen as peak 3 in the reaction mixtures with human livers (Fig. 3) was analyzed using UV and LC-MS spectra and the results were compared with those of melengestrol acetate (Fig. 4). As shown in Figs. 4A and D, metabolite M3 resulted in the UV spectra change from a maximum peak of 291 nm to 296 nm, suggesting a changed aromatic moiety in the main chemical structure. The parent ion of M3 had a molecular weight of 413 (Fig. 4B), indicating that one oxygen atom had been introduced to the melengestrol acetate molecule (Fig. 4E). Melengestrol acetate and M3 produced peaks at *m/z* 337 (Figs. 4E,4F) and *m/z* 353 (Figs. 4B,4C), respectively, commonly by losing the CH_3COO- group

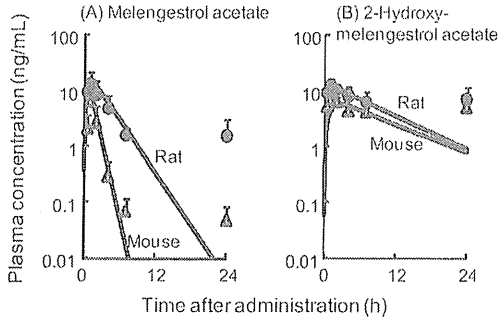

Fig. 5. Measured and estimated plasma concentrations of melengestrol acetate (A) and its metabolite 2-hydroxymelengestrol acetate (B) in rats (●) and mice (△) after single oral administration of a dose of 3 mg/kg. Data points with bars represent experimental means ± SDs obtained from four animals. The lines show chemical concentrations estimated using the PBPK model.

at the C17-position; the C2-position of the melengestrol structure was suggested to be oxidized in the MS/MS analyses of extraction of 125 *m/z* from $[M+H-59]^+$ ions, as shown in Fig. 4C. Based on several aspects of the present evidence and reported findings, peak 3 in the *in vitro* human liver microsome system was assigned as 2-hydroxymelengestrol acetate.

3.2. Human PBPK model supported by hepatic clearance experiments

To obtain detailed kinetic parameters, male rats and mice were orally administered 3.0 mg/kg of melengestrol acetate (the no-observed-adverse-effect level). Fig. 5 shows the mean levels of melengestrol acetate and 2-hydroxylated metabolites in plasma from rats and mice. Melengestrol acetate was absorbed rapidly and cleared rapidly (Fig. 5A), and its 2-hydroxylated metabolite was detected *in vivo* under the present conditions. Based on these *in vivo* experiments, the kinetic parameters for melengestrol acetate and 2-hydroxymelengestrol acetate in rats and mice were calculated and are shown in Table 2. Consequently, the final parameters such as the hepatic intrinsic clearance ($CL_{h,int}$), the volume of the systemic circulation (V_1), and the absorption rate constant (k_a) for the rat and mouse PBPK models (consisting essentially of a chemical receptor compartment, a metabolizing compartment, and a central compartment, Fig. 2) were obtained as described in the Materials and methods section. By solving the rat and mouse PBPK models, the plasma concentration curves of melengestrol acetate and its 2-hydroxymetabolite were created; the resulting estimated *in silico* concentration curves of melengestrol acetate and 2-hydroxymelengestrol acetate are shown with the *in vivo* experimental data in Figs. 5A and B.

To confirm the formation of metabolites other than 2-hydroxymelengestrol acetate, 10- and 30-mg/kg doses of melengestrol acetate were administered to control mice (Fig. 6). The three metabolites shown in the *in vitro* systems (Fig. 3) were also detected and measured in *in vivo* control mice experiments after single oral doses of 10 and 30 mg/kg (Fig. 6). To perform a toxicokinetic analysis for the melengestrol acetate and metabolites, chimeric mice were administered a dose of 100 mg/kg of melengestrol acetate in a common ratio of 3 (Fig. 7). In chimeric mice with humanized liver, plasma concentrations of melengestrol acetate (Fig. 7A), but not those of 2-hydroxymelengestrol acetate (Fig. 7D), were significantly different ($p < 0.01$) from those in control mice. By running the mouse PBPK modeling system, measured apparent maximum plasma concentrations seemed to be high because of some apparent overdosing, but the limited elimination rate between 7 h and 24 h after the treatment could be estimated with this mouse PBPK model. These observed data at 24 h were higher than the predicted curves partly because of possible enterohepatic circulation of melengestrol acetetate. According to the algometric scaling method and the obtained values shown in Table 2, the human PBPK model for melengestrol acetate and its main metabolite was set up based on the rat PBPK model. Chimeric mice with humanized liver had a relatively slow elimination curve for melengestrol acetate, and the experimental data could be reasonably estimated by the human PBPK model under the linear assumption, as shown in Fig. 7A.

Fig. 8 indicates the estimated plasma concentrations after repeated oral administration of melengestrol acetate (3.0 mg/kg) using the PBPK models for rats, mice, and humans. The maximum concentrations of melengestrol acetate were estimated to be approximately 10 ng/mL in rats, mice, and humans. When daily

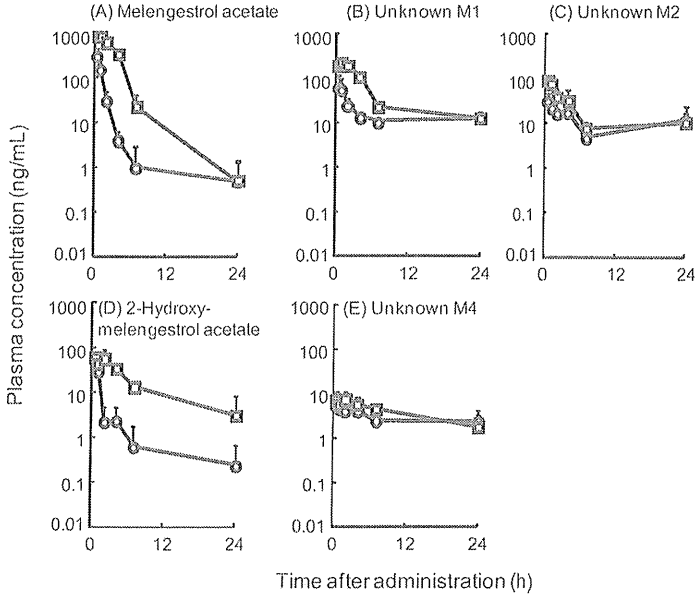

Fig. 6. Measured plasma concentrations of melengestrol acetate (A) and its four metabolites (B–E) in control mice after single oral doses of 10 mg/kg (○) and 30 mg/kg (□). See the Fig. 3 legend for information on the unknown metabolites.

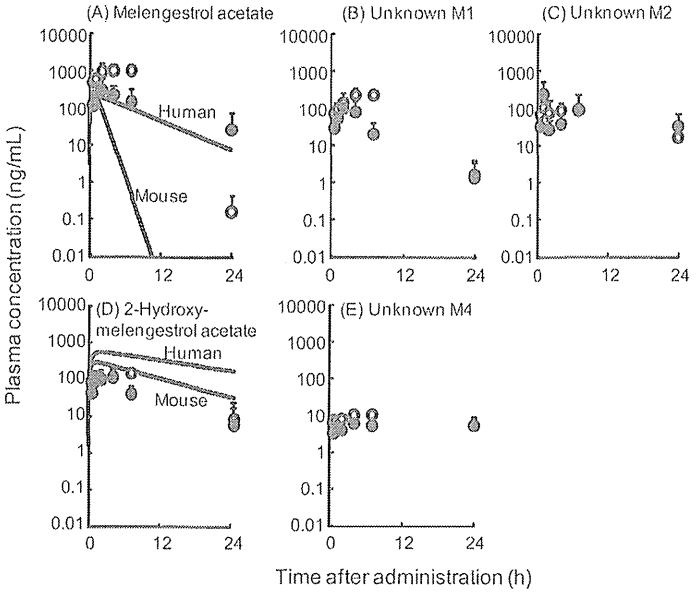

Fig. 7. Measured plasma concentrations of melengestrol acetate (A) and its metabolites (B–E) in mice with (●) and without (○) humanized liver and concentrations for humans and mice estimated using PBPK models (lines) after single oral administration of a dose of 100 mg/kg. Data points with bars represent experimental means ± SDs obtained from four animals. The lines in panels A and D show chemical plasma concentrations in mice and humans estimated using PBPK models. In panel A, B, and E, the mean concentrations for chimeric mice with humanized liver at 2 h, 4 h, and/or 7 h after administration were significantly lower ($p < 0.05$) than those in control mice by two-way ANOVA with Bonferroni post tests.

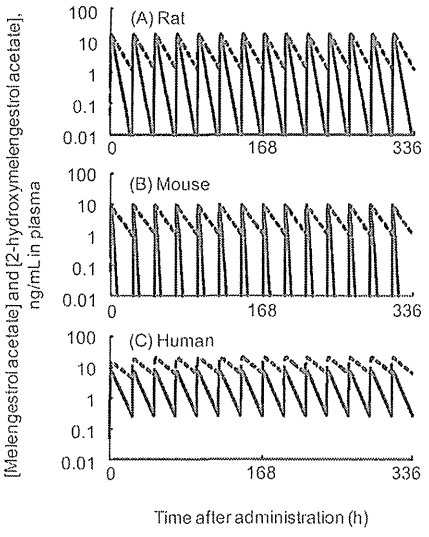

Fig. 8. Melengestrol acetate and 2-hydroxymelengestrol acetate concentrations estimated using the PBPK model in rats (A), mice (B), and humans (C) after multiple oral administrations (3.0 mg/kg per day). Melengestrol acetate (solid line) and 2-hydroxymelengestrol acetate (dashed line) accumulation were estimated after multiple doses.

administration of melengestrol acetate for 14 days was modeled, metabolite accumulations were evident in rats, mice, and humans (Fig. 8); however, melengestrol acetate accumulation was found only in humans using the present PBPK models (Fig. 8C).

4. Discussion

Melengestrol acetate has a higher affinity for the progestin receptor than progesterone does (Bauer et al., 2000; Pfaffl et al., 2002). Although several metabolites of melengestrol acetate, possibly containing mono- and dihydroxylated moieties, were noted in an LC profile of reactions mediated by rat liver microsomes (Metzler and Pfeiffer, 2001), none of them was adequately characterized with regard to chemical structure. Three major but unidentified metabolites of melengestrol acetate have been indicated to have less affinity for the progestin receptor than progesterone or melengestrol acetate do (Bauer et al., 2000). High-resolution LC analysis of some commercial melengestrol acetate samples has suggested the presence of several impurities in the form of metabolites capable of inducing apoptosis in the cell systems (Bauer et al., 2000). In the present study, the major metabolite of melengestrol acetate (peak 3 in Fig. 3), which was efficiently formed by human P450 3A4 (Table 4) and was mainly metabolized in human liver microsomes (Table 3), was identified for the first time as 2-hydroxymelengestrol acetate by a series of structural analysis studies, as shown in Fig. 4. We were unable to fully determine the structures of the other currently unidentified di- or monohydroxymelengestrol acetate metabolites; however, our preliminary UV spectra and MS/MS analyses (data not shown), together with limited literature information (Cooper et al., 1967; Elce et al., 1967; Metzler and Pfeiffer, 2001; Joint FAO/WHO Expert Committee, 2009), are consistent with tentative identifications of M1, M2, and M4 as 2,15-dihydroxymelengestrol acetate, 15-hydroxymelengestrol acetate, and 6-hydroxymethyl-melengestrol acetate respectively. Consequently, melengestrol acetate may be deactivated by the oxidative biotransformations proposed in the literature and suggested by the results of the present study, but the metabolites formed are still hormonally and biologically active substances that will be present in the edible tissues of farm animals and, as a result, in human bodies.

It is generally accepted that PBPK modeling is useful for understanding the relationships between chemical exposure and the resulting concentrations in body fluids (Fig. 1). However, the multiple compartments and many complicated equations found in traditional PBPK modeling cause severe difficulties when applying the model. Simplified PBPK modeling was adopted in the present study (Fig. 2) because it can be fully evaluated and carefully considered

by other scientists, industrial users, and regulatory authorities. The present study defined a simplified PBPK model for melengestrol acetate in humans; the model was based on physiological parameters derived from the literature, coefficients derived *in silico*, metabolic parameters determined *in vitro* using relevant liver microsomes, and *in vivo* experiment-supported PBPK modeling in rats and mice (Tables 1 and 2). The developed PBPK model simply consists of three compartments for the parent compound and primary metabolite: the gut as a chemical absorption compartment for parent compound, the liver as a metabolizing compartment, and the general circulation as the central compartment (Fig. 2). In this context, it is interesting to estimate melengestrol acetate disposition in humans in future by full PBPK system such as a population-based absorption, distribution, metabolism, and excretion simulator Simcyp (Jamei et al., 2009), which is a platform and database for 'bottom-up' mechanistic modeling and simulation.

Because of the simplicity of our adopted PBPK model, a reliable human hepatic clearance value, as well as overall human PBPK parameters, could be estimated from limited experiments, i.e., oral dose administration in rats or mice and *in vitro* clearance experiments with rat, mouse, and human liver microsomes in the present study. Adjusted animal biomonitoring equivalents after melengestrol acetate was administered in mouse and rat studies were scaled to human biomonitoring equivalents using known species allometric scaling factors and human metabolic data with the simple PBPK model adopted in this study. Melengestrol acetate elimination in humans was estimated by the PBPK model to be slow compared with elimination in rodents (Fig 8). The slow drug disposition of melengestrol acetate in humans was evaluated using chimeric TK-NOG mice with humanized liver (Fig. 7). Apparent different elimination rates of melengestrol acetate in chimeric mice would not only be due to the *in vitro* humanized enzyme activity, but also other physiological and/or kinetics parameters. The simplified PBPK model for melengestrol acetate and the use of TK-NOG mice with humanized liver may also be useful for risk evaluation and for simulating plasma concentrations resulting from exposure to low doses of melengestrol acetate.

In discussions on the setting of an acceptable human daily intake level of melengestrol acetate, using the lowest-observed-adverse-effect level in rats with an uncertainty factor of 1000 has been considered (Joint FAO/WHO Expert Committee, 2009). Although difference in early elimination kinetics might have some limitations in assessment of fully chronic exposure of melengestrol acetate, together with the present results that melengestrol acetate clearance in humans may be slower than that in rodents (Fig. 8), a species difference factor in uncertainty factor should be considered in setting the uncertainty factor to take into account the possibly slower clearance in humans. To solve the question how much degree of the uncertainty factor for species difference should be recommended, it would be totally taken into consideration the results of the quantitative PBPK analysis as well as pharmacological/toxicological potential of the compound and metabolites.

5. Conclusions

A simplified PBPK model for the synthetic progesterone melengestrol acetate and its primary metabolite was developed using a combination of algorithms, *in vitro* and *in vivo* experimentation, and literature resources. According to the present PBPK analysis, melengestrol acetate is cleared more slowly from plasma in humans than in rodents. The present study indicates that simplified PBPK modeling is useful for application of the forward dosimetry approach to melengestrol acetate and to other related compounds for low chemical doses such as those at the no-observed-adverse-effect level.

Conflict of interest statement

The authors declare that there are no conflicts of interest.

Acknowledgments

This work was supported in part by The Food Safety Commission of Japan; the Ministry of Education, Culture, Sports, Science and Technology of Japan; and JCIA's LRI program.

Appendix A

The liver–plasma concentration ratio ($K_{p,h}$) and the ratio of the blood to plasma concentration (R_b) were calculated using the following equations (Poulin and Theil, 2002):

$$K_{p,h} = \frac{0.02289 \cdot P + 0.72621}{0.00396 \cdot P + 0.960581} \cdot \frac{f_{u,p} + 1}{2} \quad (A1)$$

$$R_b = 0.45 \cdot (K_b \cdot f_{u,p} - 1) + 1 \quad (A2)$$

$$\log K_b = 0.617 \cdot \log\left(\frac{1 - f_{u,p}}{f_{u,p}}\right) + 0.208 \quad (A3)$$

where P is the water-octanol partition ratio [estimated from the computer-calculated logP as neutral (clogP)] and $f_{u,p}$ is the plasma unbound fraction. Hepatic interstitial fluid-to-plasma concentration ratios of albumin, globulins, and lipoproteins were assumed to be 0.5.

The initial parameter value of the hepatic intrinsic clearance ($CL_{h,int}$) used to execute the fitting calculation of the PBPK model with WinNonlin software was derived as follows. First, the hepatic clearance (CL_h) was estimated:

$$CL_h = \frac{Q_h \cdot Dose - Q_h \cdot AUC \cdot CL_r}{Dose + Q_h \cdot AUC} \quad (A4)$$

where AUC and Q_h are the area under the plasma concentration curve and the hepatic blood flow rate of the systemic circulation to the hepatic compartment, respectively, and CL_r is the renal clearance. In this study, we assumed that the fraction absorbed (F_a) × intestinal availability (F_g) = 1.0; then, the bioavailability (F) was calculated:

$$F = F_h = 1 - \frac{CL_h}{Q_h} \quad (A5)$$

where F_h is the fraction unmetabolized in the liver. The initial value of $CL_{h,int}$ was estimated from Eq. (A6), where CL_h was evaluated using the total clearance (CL_{tot}) with the distribution volume (V_d) and elimination constant (k_{el}) from Eqs. (A7), (A8):

$$CL_{h,int} = \frac{R_b}{f_{u,p}} \cdot \frac{Q_h \cdot CL_h}{Q_h - CL_h} \quad (A6)$$

$$CL_h = CL_{tot} - CL_r \quad (A7)$$

$$CL_{tot} = V_d \cdot k_{el} \quad (A8)$$

References

Amidon, G.L., Sinko, P.J., Fleisher, D., 1988. Estimating human oral fraction dose absorbed: a correlation using rat intestinal membrane permeability for passive and carrier-mediated compounds. Pharm. Res 5, 651–654.

Bauer, E.R., Daxenberger, A., Petri, T., Sauerwein, H., Meyer, H.H., 2000. Characterisation of the affinity of different anabolics and synthetic hormones to the human androgen receptor, human sex hormone binding globulin and to the bovine progestin receptor. APMIS 108, 838–846.

Clewell, H.J., Gentry, P.R., Covington, T.R., Sarangapani, R., Teeguarden, J.G., 2004. Evaluation of the potential impact of age- and gender-specific pharmacokinetic differences on tissue dosimetry. Toxicol. Sci. 79, 381–393.

Cooper, J.M., Elce, J.S., Kellie, A.E., 1967. The metabolism of melengestrol acetate. Biochem. J. 104, 57P–58P.
Edwards, S.W., Preston, R.J., 2008. Systems biology and mode of action based risk assessment. Toxicol. Sci. 106, 312–318.
Elce, J.S., Cooper, J.M., Kellen, E., 1967. Plasma levels of melengestrol acetate. Biochem. J. 104, 58P–59P.
Emoto, C., Murayama, N., Rostami-Hodjegan, A., Yamazaki, H., 2009. Utilization of estimated physicochemical properties as an integrated part of predicting hepatic clearance in the early drug-discovery stage: Impact of plasma and microsomal binding. Xenobiotica 39, 227–235.
Gargas, M.L., Andersen, M.E., Teo, S.K.O., Batra, R., Fennell, T.R., Kedderis, G.L., 1995. A physiologically based dosimetry description of acrylonitrile and cyanoethylene oxide in the rat. Toxicol. Appl. Pharmacol. 134, 185–194.
Hasegawa, M., Kawai, K., Mitsui, T., Taniguchi, K., Monnai, M., Wakui, M., Ito, M., Suematsu, M., Peltz, G., Nakamura, M., Suemizu, H., 2011. The reconstituted 'humanized liver' in TK-NOG mice is mature and functional. Biochem. Biophys. Res. Commun. 405, 405–410.
Jamei, M., Marciniak, S., Feng, K., Barnett, A., Tucker, G., Rostami-Hodjegan, A., 2009. The Simcyp population-based ADME simulator. Expert Opin. Drug Metab. Toxicol. 5, 211–223.
Joint FAO/WHO Expert Committee, 2009. Evaluation of certain veterinary drug residues in food. World Health Organ Tech. Rep. Ser. 1–134.
Kato, M., Shitara, Y., Sato, H., Yoshisue, K., Hirano, M., Ikeda, T., Sugiyama, Y., 2008. The quantitative prediction of CYP-mediated drug interaction by physiologically based pharmacokinetic modeling. Pharm. Res. 25, 1891–1901.
Lauderdale, J.W., Goyings, L.S., Krzeminski, L.F., Zimbelman, R.G., 1977. Studies of a progestogen (MGA) as related to residues and human consumption. J. Toxicol. Environ. Health 3, 5–33.
McLanahan, E.D., El-Masri, H.A., Sweeney, L.M., Kopylev, L.Y., Clewell, H.J., Wambaugh, J.F., Schlosser, P.M., 2012. Physiologically based pharmacokinetic model use in risk assessment – why being published is not enough. Toxicol. Sci. 126, 5–15.
Metzler, M., Pfeiffer, E., 2001. Genotoxic potential of xenobiotic growth promoters and their metabolites. APMIS 109, 89–95.
Murayama, N., Kaneko, N., Horiuchi, K., Ohyama, K., Shimizu, M., Ito, K., Yamazaki, H., 2009. Cytochrome P450-dependent drug oxidation activity of liver microsomes from microminipigs, a possible new animal model for humans in non-clinical studies. Drug Metab. Pharmacokinet. 24, 404–408.
Patterson, D.J., Kiracofe, G.H., Stevenson, J.S., Corah, L.R., 1989. Control of the bovine estrous cycle with melengestrol acetate (MGA): a review. J. Anim. Sci. 67, 1895–1906.
Perry, G.A., Welshons, W.V., Bott, R.C., Smith, M.F., 2005. Basis of melengestrol acetate action as a progestin. Domest. Anim. Endocrinol. 28, 147–161.
Pfaffl, M.W., Daxenberger, A., Hageleit, M., Meyer, H.H., 2002. Effects of synthetic progestagens on the mRNA expression of androgen receptor, progesterone receptor, oestrogen receptor alpha and beta, insulin-like growth factor-1 (IGF-1) and IGF-1 receptor in heifer tissues. J. Vet. Med. A Physiol. Pathol. Clin. Med. 49, 57–64.
Poulin, P., Theil, F.P., 2002. Prediction of pharmacokinetics prior to in vivo studies. 1. Mechanism-based prediction of volume of distribution. J. Pharm. Sci. 91, 129–156.
Schiffer, B., Daxenberger, A., Meyer, K., Meyer, H.H., 2001. The fate of trenbolone acetate and melengestrol acetate after application as growth promoters in cattle: environmental studies. Environ. Health Persp. 109, 1145–1151.
Stephany, R.W., 2010. Hormonal growth promoting agents in food producing animals. Handb. Exp. Pharmacol., 355–367.
Sweeney, L.M., Gargas, M.L., Strother, D.E., Kedderis, G.L., 2003. Physiologically based pharmacokinetic model parameter estimation and sensitivity and variability analyses for acrylonitrile disposition in humans. Toxicol. Sci. 71, 27–40.
Takano, R., Murayama, N., Horiuchi, K., Kitajima, M., Kumamoto, M., Shono, F., Yamazaki, H., 2010. Blood concentrations of acrylonitrile in humans after oral administration extrapolated from *in vivo* rat pharmacokinetics, *in vitro* human metabolism, and physiologically based pharmacokinetic modeling. Regul. Toxicol. Pharmacol. 58, 252–258.
Wild, C.P., 2005. Complementing the genome with an "exposome": the outstanding challenge of environmental exposure measurement in molecular epidemiology. Cancer Epidemiol. Biomarkers Prev. 14, 1847–1850.
Yamazaki, H., Horiuchi, K., Takano, R., Nagano, T., Shimizu, M., Kitajima, M., Murayama, N., Shono, F., 2010. Human blood concentrations of cotinine, a biomonitoring marker for tobacco smoke, extrapolated from nicotine metabolism in rats and humans and physiologically based pharmacokinetic modeling. Int. J. Environ. Res. Public Health 7, 3406–3421.
Yamazaki, H., Shimizu, M., Nagashima, T., Minoshima, M., Murayama, N., 2006. Rat cytochrome P450 2C11 in liver microsomes involved in oxidation of anesthetic agent propofol and deactivated by prior treatment with propofol. Drug Metab. Dispos. 34, 1803–1905.
Yamazaki, H., Suemizu, H., Igaya, S., Shimizu, M., Shibata, M., Nakamura, M., Chowdhury, G., Guengerich, F.P., 2011. *In vivo* formation of a glutathione conjugate derived from thalidomide in humanized uPA-NOG mice. Chem. Res. Toxicol. 24, 287–289.
Yamazaki, H., Suemizu, H., Shimizu, M., Igaya, S., Shibata, N., Nakamura, N., Chowdhury, G., Guengerich, F.P., 2012. *In vivo* formation of dihydroxylated and glutathione conjugate metabolites derived from thalidomide and 5-hydroxythalidomide in humanized TK-NOG mice. Chem. Res. Toxicol. 25, 274–276.

Effect of *in vivo* administration of reprogramming factors in the mouse liver

AKIRA TOMOKUNI[1], HIDETOSHI EGUCHI[1], HIROMITSU HOSHINO[1], DYAH LAKSMI DEWI[1], SHINPEI NISHIKAWA[1], YOSHIHIRO KANO[1], NORIKATSU MIYOSHI[1], ARINOBU TOJO[2], SEIICHIRO KOBAYASHI[2], NORIKO GOTOH[3], KUNIHIKO HINOHARA[3], NOEMI FUSAKI[4], TOSHIYUKI SAITO[5], HIROSHI SUEMIZU[6], HIROSHI WADA[1], SHOGO KOBAYASHI[1], SHIGERU MARUBASHI[1], MASAHIRO TANEMURA[1], YUICHIRO DOKI[1], MASAKI MORI[1], HIDESHI ISHII[1] and HIROAKI NAGANO[1]

[1]Department of Gastroenterological Surgery, Osaka University Graduate School of Medicine, Suita, Osaka 565-0871; Divisions of [2]Molecular Therapy and [3]Systems Biomedical Technology, Institute of Medical Science, University of Tokyo, Minato-ku, Tokyo 108-8639; [4]DNAVEC Corporation, Tsukuba, Ibaraki 300-2611; [5]Transcriptome Profiling Group, National Institute of Radiological Sciences, Inage-ku, Chiba 263-8555; [6]Biomedical Research Department, Central Institute for Experimental Animals, Miyamae, Kawasaki, Kanagawa 216-0001, Japan

Received January 25, 2013; Accepted May 14, 2013

DOI: 10.3892/ol.2013.1418

Abstract. Cancer is initiated by the transformation of stem cells or progenitor cells via a dedifferentiation process that leads to cancer stem cells; however, the process involves the activation of growth-promoting oncogenes and the inactivation of growth-constraining tumor suppressor genes. The introduction of defined factors, such as those encoded by *c-Myc*, *Sox2*, *Oct3/4* and *Klf4*, in normal somatic cells results in their dedifferentiation into induced pluripotent stem (iPS) cells. We previously reported that these defined factors induced the development of induced multipotent cancer (iPC) cells from gastrointestinal cancer cells by reducing tumor aggressiveness. Previous studies indicated that although reprogramming may be facilitated by *p53* inhibition, gain-of-function oncogenic mutations in *p53* and oncogenic mutations in *Kras*-stimulated tumorigenic activity, and their roles *in vivo* are imperfectly understood. Hence, in the present study, the effect of direct injection of a Sendai virus (SeV) vector encoding four defined factors *in vivo* was studied using various backgrounds of transgenic and knockout mice, and was compared with that of direct injection of microRNAs (miRNAs) diluted with cationic lipid. The *in vivo* imaging data revealed transformation hot spots for *p53* deficiency or conditional activation of mutant *Kras*, and the sizes were concordant with those in immunodeficient NOD/SCID and uPA-NOG mice, as well as larger compared with those in the control mice. Overall, the present data on *in vivo* reprogramming indicated that *Kras* activation may facilitate the effect of cellular reprogramming in normal liver cells, and the effect of *Kras* activation is more apparent than that of tumor suppressor *p53* deficiency. The results also revealed that immunodeficiency may increase the effect of reprogramming, presumably by blocking the immunosurveillance of transformed cells. These findings provide a rationale for further studies to develop a therapeutic approach involving direct *in vivo* reprogramming.

Correspondence to: Dr Hideshi Ishii or Dr Hiroaki Nagano, Department of Gastroenterological Surgery, Osaka University Graduate School of Medicine, 2-2 Yamadaoka, Suita, Osaka 565-0871, Japan
E-mail: hishii@cfs.med.osaka-u.ac.jp
E-mail: hnagano@gesurg.med.osaka-u.ac.jp

Abbreviations: iPS cells, induced pluripotent stem cells; ES cells, embryonic stem cells; iPC cells, induced multipotent cancer cells; 5-FU, 5-fluorouracil; SeV, Sendai virus; miRNA, microRNA; NOD/SCID mice, NOD.CB17-*Prkdc*^{scid}/J mice; NOG mice, NOD.Cg-*Prkdc*^{scid} *Il2rg*^{tm1Sug}/Jic mice; uPA, urokinase-type plasminogen activator; MMTV, mouse mammary tumor virus; LTR, long terminal repeat

Key words: Kras, *p53*, reprogramming, differentiation, liver

Introduction

The discovery that complete cellular reprogramming may be achieved by introducing the defined transcription factors *c-Myc*, *Sox2*, *Oct3/4* and *Klf4* into terminally differentiated somatic fibroblasts of mouse and human origins was an important breakthrough (1,2). The generation of induced pluripotent stem (iPS) cells by the introduction of defined factors, which are generally expressed in embryonic stem (ES) cells, results in the reconstitution of organs in chimeric mice and contributes to the regeneration of human tissues (3). We previously showed that gastrointestinal cancer cells acquired multipotential differentiation ability upon the introduction of defined factors; the gene expression profiles of mesodermal and ectodermal cells appeared in gastrointestinal cancer cells of endodermal origin

[termed induced multipotent cancer (iPC) cells] (4). Whether the iPC cells were generated via a state of pluripotency remains to be investigated, although the iPC cells expressed ES-like genes and possessed the ability to differentiate from cells of endodermal origin into other endoderm and mesoderm lineages (4). Notably, *in vitro* differentiation resulted in sensitization to therapeutic reagents such as vitamins A and D and the chemotherapeutic agent 5-fluorouracil (5-FU), as well as reduced tumorigenicity, suggesting that altering the cancer cell lineage through reprogramming *in vivo* may be a promising concept for novel and efficient cancer therapy (4). However, at present, there are a limited number of studies concerned with reprogramming *in vivo*, and thus the mechanism involved in reprogramming *in vivo* remains unknown.

Epithelial tumor tissues are composed of various types of mesenchymal cells, such as myofibroblasts, fibroblasts, endothelial cells, lymphocytes, monocytes and macrophages, certain of which are known to be components of a microenvironment (niche). These components are involved in tumorigenesis at the early stages, support cancers cells and provide resistance against exposure to chemotherapeutic reagents. Overall, although it is assumed that mesenchymal cells are important in the process of reprogramming in the complex system *in vivo*, no investigations on how reprogramming factors affect the mesenchymal components have been conducted. To assess this, the effect of direct injection of a Sendai virus (SeV) vector encoding four defined factors into the liver was studied using transgenic and knockout mice with various genetic backgrounds, and the effect was compared with that of direct injection of microRNAs (miRNAs) diluted with cationic lipid. The *in vivo* bioluminescence imaging data revealed transformation hot spots for *p53* (also known as *TP53* in humans and *Trp53* in mice) deficiency or conditional activation of mutant *Kras*, and the sizes were consistent with those in immunodeficient NOD.CB17-*Prkdc*^{scid}/J (NOD/SCID) mice and NOD.Cg-*Prkdc*^{scid} *Il2rg*^{tm1Sug}/Jic (NOG) mice expressing transgenic urokinase-type plasminogen activator (*uPA*) in the liver (uPA-NOG), as well as larger compared with those in the control mice. The present results suggested that the effect of reprogramming-based, novel therapeutic approaches was enhanced by *Kras* activation. The effect was more apparent with *Kras* activation than with tumor suppressor *p53* deficiency, suggesting a distinct role for the *Kras* pathway in direct reprogramming in the liver. Furthermore, immunodeficiency may increase the effect of reprogramming, presumably by blocking the immunosurveillance of transformed cells.

Subjects and methods

Experimental animals. NOD/SCID mice were purchased from Charles River Japan (Osaka, Japan). All animal experiments were performed with approval from the Animal Experiments Committee of Osaka University. The NOD/SCID mice lack B cells, T cells and the complement system, and possess severely reduced natural killer (NK) cells. More severely immunodeficient uPA-NOG mice were produced by extra-uterine fertilization, resulting in zygotes that expressed transgenic *uPA* in the liver; the extracellular matrix in the liver was modified to activate the hemolytic system, which facilitated xenogeneic engraftment or growth of transformed cells in the present experiment in mice with an immunodeficient background (5). Heterozygous B6.129S4-*Kras*^{tm4Tyj}/J mice (Jackson Laboratory, Bar Harbor, ME, USA), which carry an allele with the most common point mutation whose expression is blocked by the presence of a loxP-flanked stop codon in the ROSA loci, were crossed with B6129-Tg(MMTV-Cre)4Mam/J mice (Jackson Laboratory), which express P1 Cre recombinase under the control of the mouse mammary tumor virus (MMTV) long terminal repeat (LTR) promoter. The MMTV LTR promoter directs a widespread pattern of expression to produce CMV-Cre/*Kras*^{mut} mice; and when expressed in B6.Cg-Tg(Alb-Cre)21Mgn/J mice (Jackson Laboratory), is efficient in achieving liver-specific recombination to produce Alb-Cre/*Kras*^{mut} mice. B6.129S2-*Trp53*^{tm1Tyj}/J mice (Jackson Laboratory), from which a mutant allele was produced by a targeted neo insertion into the *p53* locus, were mated with STOCK Tg(Nanog-GFP, Puro)1 Yam mice, which express the green fluorescent protein under the control of the *Nanog* gene promoter (RIKEN BioResource Center, Tsukuba, Japan), to produce Nanog-GFP/*Trp53*$^{+/-\,(KO)}$ mice. Overall, two immunodeficient mice were used in the experiments, NOD/SCID and uPA-NOG, as well as CMV-Cre/*Kras*^{mut}, Alb-Cre/ *Kras*^{mut} and Nonog-GFP/*Trp53*^{KO} mice. miRNAs were also used to assess the effect.

In vivo administration of viral construct mixture. SeV vectors replicate in the form of negative-sense single-stranded RNA in the cytoplasm of infected cells and do not undergo a DNA phase or integrate into the host genome (6). It was shown that the efficient induction of transgene-free human pluripotent stem cells was achieved using a vector based on SeV, an RNA virus that does not integrate into the host genome; iPS induction could be achieved by the SeV-mediated gene-transfer introduction of the defined transcription factors *c-Myc*, *Sox2*, *Oct3/4* and *Klf4* from terminally differentiated somatic cells (7). A viral construct mixture consisting of: i) 5 μl lentiviral vector and ii) SeV vectors (2.5 μl per each transcription factor) or 10 μl miRNAs was prepared. Co-transfection of the lentiviral luciferase gene was performed to trace the cell populations in which the genes were introduced. The SeV vectors were mixed according to the transcription factors to be introduced, such as SeV vectors encoding *c-Myc*, *Sox2*, *Oct3/4* and *Klf4* (MSOK); *Sox2*, Oct4 and *Klf4* (SOK); or *c-Myc* alone (M). With regard to miRNAs, 60 pmol of double-stranded mature miRNAs (20 pmol of mmu-miR-200c; 5 pmol of mmu-miR-302a, -302b, -302c and -302d; and 10 pmol of mmu-miR-369-3p and -5p) was diluted with 10 μl siPORT (Ambion, Austin, TX, USA). Median laparotomy was performed in each mouse under sevoflurane anesthesia and the viral construct mixture was directly injected into the median lobe of the liver.

In vivo imaging. To trace the behavior of the injected viral construct, the animals were examined at days 14, 21 and 28 using the IVIS Lumina II imaging system (Caliper Life Sciences, Hopkinton, MA, USA) (Fig. 1). Each mouse received luciferin intraperitoneally at 4 mg/kg and was then anesthetized with 2% isoflurane; the mice were left undisturbed for 10 min thereafter. Subsequently, the mice were imaged under the following conditions: Exposure, 2 min; f-stop, 1; binning,

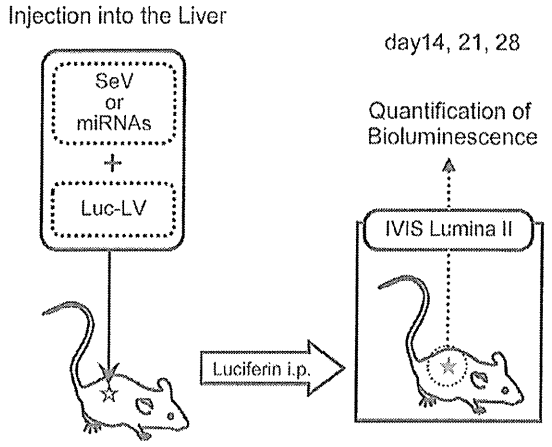

Figure 1. Schematic representation of the study. The immunodeficient mice, NOD/SCID and uPA-NOG, as well as the CMV-Cre/*Kras*^{mut}, Alb-Cre/*Kras*^{mut} and Nonog-GFP/*Trp53*^{KO} mice, received injection of the Sendai virus (SeV) vector encoding transcription factors (including *c-Myc*, *Sox2*, *Oct3/4* and *Klf4*) into the livers by laparotomy. As a control, microRNAs (miRNAs) diluted with cationic lipid were injected. To trace the effect, the lentiviral luciferase gene (Luc-LV) was co-injected. At the indicated days after injection, the mice received administration of luciferin intraperitoneally and the signal was assessed using the IVIS Lumina II system.

medium; field of view, 12.5 cm. Bioluminescence values were calculated as photons/s/cm^2/sr in the region of interest.

Results

Immunodeficient mice. In the NOD/SCID mice, the luciferase-positive area was detected 14, 21 and 28 days following the injection of viral construct mixture (Fig. 2A). The mice showed no apparent health problems. The uPA-NOG mice showed a more apparent luciferase-positive area, which was negative at day 14, but positive at day 21 and more apparent compared with day 28. The data suggested that liver-specific modification of the extracellular matrix under immunodeficient conditions may induce a more apparent effect. By contrast, direct injection of miRNAs indicated that the luciferase-positive area was relatively small in NOD/SCID mice, but was increased in uPA-NOG mice at day 28 (Fig. 2B), suggesting that the effects of the SeV vector infection were more apparent than the *in vivo* transfection of miRNAs, and that the extracellular structure of the liver and immunosurveillance may alter the effect.

Oncogenic Kras activation in mice. To investigate the effect of oncogenic *Kras* activation in mice, CMV-Cre/*Kras*^{mut} mice were produced, which expressed the oncogenic *Kras* allele with a point mutation (G12D; Fig. 3A). The luciferase-positive area was detected at days 14, 21 and 28. Another luciferase-positive area, in the right thoracic region, was also noted. The data suggested that oncogenic *Kras* may be involved in accelerating the cellular reprogramming process. The effect was marginal in miRNA-injected mice (Fig. 3B), presumably due to the relatively low gene transfection efficiency compared with SeV vector injection.

To clarify whether hepatocytes or non-hepatocytes (such as mesenchymal cells) in the liver were involved in the effect, Alb-Cre/*Kras*^{mut} mice were produced and SeV vector encoding *c-Myc*, *Sox2*, *Oct3/4* and *Klf4* (MSOK) was directly injected (Fig. 3C). The luciferase-positive area was limited compared with that of CMV-Cre/*Kras*^{mut} mice. The data were similar following the injection of SeV vector encoding *Sox2*, *Oct3/4* and *Klf4* but not *c-Myc* (SOK; Fig. 3D), suggesting that Alb-positive hepatocytes were unlikely to be targets of cellular reprogramming.

To study the effect of *c-Myc* in oncogenic *Kras* mutation, SeV vector encoding *c-Myc* (M) was injected into CMV-Cre/*Kras*^{mut} mice (Fig. 3E). The luciferase-positive area was detected at days 14, 21 and 28, while the injection of SeV vector encoding *c-Myc*, *Sox2*, *Oct3/4* and *Klf4* (MSOK) into the control CMV-Cre mice showed a similar luciferase-positive area (Fig. 3F). The data suggested that the oncogenic *Kras* mutation was compatible with the administration of *Sox2*, *Oct3/4* and *Klf4*.

Tumor suppressor p53-deficient mice. Previous studies have shown that the inhibition or absence of *p53* significantly increased the reprogramming efficiency of somatic cells to reach a pluripotent state (8-10). Further studies have demonstrated that decreasing the level of the tumor suppressor *p53* protein enables the development of iPS cells from murine fibroblasts; these iPS cells are capable of generating germline-transmitting chimeric mice, suggesting that *p53* may not be necessary for reprogramming. The inhibition or absence of *p53* significantly increases the reprogramming efficiency of human somatic cells (8-10).

To assess the effect of this observation *in vivo*, Nanog-GFP/*Trp53*^{KO} mice were produced and infected with SeV vector encoding *c-Myc*, *Sox2*, *Oct3/4* and *Klf4* (Fig. 3G). Although the efficiency was low, it was possible to detect the luciferase-positive area at days 14, 21 and 28. The administration of miRNAs did not produce a luciferase-positive area, suggesting that the efficiency of this approach was low or undetectable (Fig. 3H). The data showed that although the effect of *p53* was significant in cellular reprogramming, its effect in direct reprogramming in the liver was limited.

Discussion

Although there is little knowledge concerning the mechanism of reprogramming *in vivo*, it is known that certain types of gene alterations have significant effects on cellular reprogramming *in vitro*. For example, the absence of *p53*, which is critical in epithelial tumors, increases the efficiency of iPS cell generation (8-10). We previously demonstrated that the reprogramming efficiency was enhanced by co-transfection of key tumor suppressor gene mutants (11, data not shown). The results support the theory that mutations involved in DNA contact may be critical in the efficiency of iPS generation, and suggest two roles for *p53* mutations in reprogramming. Structural mutations may contribute to the maintenance of genomic stability, while DNA contact mutations define the downstream target genes, which may be distinct from wild-type *p53* function. Moreover, in a further reprogramming study using other cancer cells with gain-of-function mutations, such as *p53*R175H and *Kras*^{G12D}, we demonstrated the multipotency of differentiation and temporal suppression of tumorigenicity.

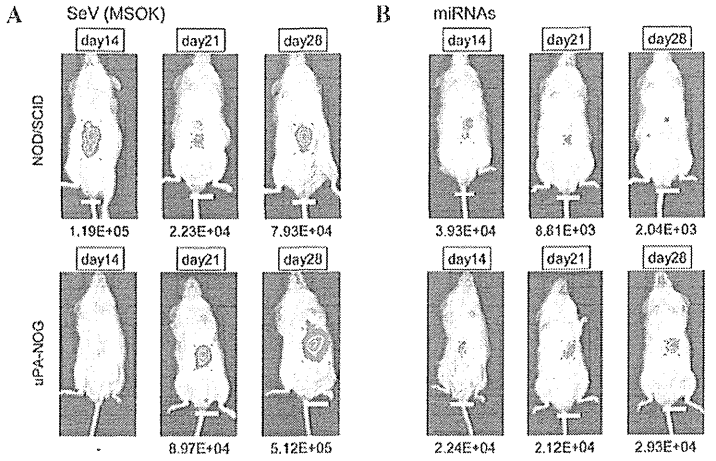

Figure 2. Immunodeficient mice with reprogramming factors. Two immunodeficient mice, NOD/SCID and uPA-NOG, received four factors (*c-Myc*, *Sox2*, *Oct3/4 and Klf4*; MSOK) or microRNAs (miRNAs). At the indicated days after injection, the mice received luciferin and the signal was assessed using the IVIS Lumina II system. The colored area represents the luciferase-positive area and its bioluminescence was quantified as shown below the respective images. SeV, Sendai virus.

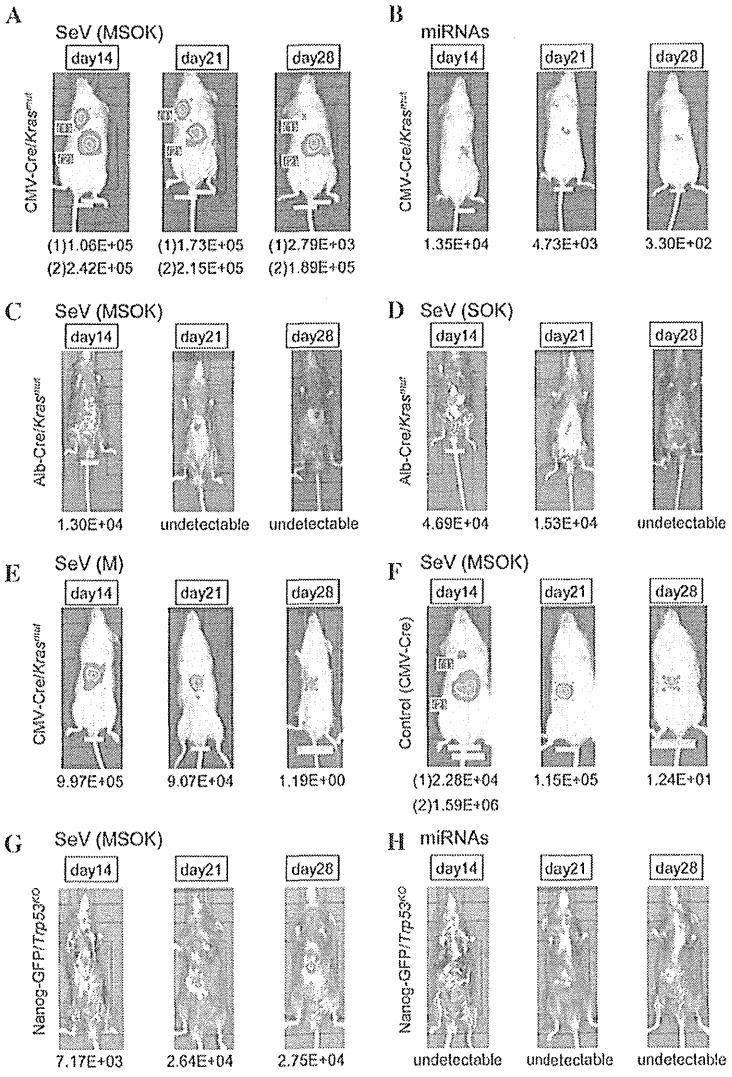

Figure 3. Oncogenic *Kras*-expressing mice and tumor suppressor *p53*-deficient mice with reprogramming factor(s) or microRNAs (miRNAs). (A-F) Two conditional knockout mice, CMV-Cre/*Kras*^{mut} and Alb-Cre/*Kras*^{mut} and the control CMV-Cre mice received four factors (*c-Myc*, *Sox2*, *Oct3/4 and Klf4*; MSOK), three factors (*Sox2*, *Oct3/4* and *Klf4*; SOK), one factor (*c-Myc*; M) or miRNAs. Tumor suppressor *p53*-deficient mice received (G) four factors (MSOK), or (H) miRNAs. At the indicated days after injection, the mice received luciferin and the signal was assessed using the IVIS Lumina II system. The colored area represents the luciferase-positive area and its bioluminescence was quantified as shown below the respective images. SeV, Sendai virus.

However, the cells subsequently resumed growth in long-term culture (>2 months) and also showed increased tumorigenicity. After iPS factor-mediated reprogramming, the expression of ES-like genes, with the exception of activated endogenous *c-Myc*, was downregulated in long-term cultures of iPC cells derived from cholangiocellular carcinoma HuCC-T1 cells with gain-of-function mutations. This suggests a role for such oncogenic mutations in the reactivation of a malignant phenotype in long-term culture, presumably via the accumulation of further mutations or increased genomic instability during *in vitro* culture (11).

The present study showed that the following factors were involved in the efficiency of the causal effects due to directly administered reprogramming factors in the liver *in vivo*: i) immunodeficiency; ii) extracellular components such as *uPA*; and iii) activation of oncogenic *Kras* in mesenchymal cells.

Severely immunodeficient NOG mice are utilized as recipients for human tissue transplantation, which produces chimeric mice with various types of human tissue. In the present study, uPA-NOG mice were used. Human hepatocytes injected into uPA-NOG mice repopulated the recipient livers with human cells, and the uPA-NOG model has a number of advantages over previously produced chimeric mouse models of the human liver (5). The immunodeficient condition facilitates this process by the elimination of transformed cells. In the present study, uPA-NOG mice showed larger luciferase-positive areas in comparison with NOD/SCID mice, suggesting that the extracellular matrix has a critical effect on reprogramming. Furthermore, the tissues were examined and an irregular arrangement of hepatocytes was observed, although no cancerous cells or teratoma were detected, suggesting that the cells directly affected by reprogramming factors *in vivo* may be altered or adapted in tissues with a supportive surrounding microenvironment.

Oncogenic *Kras* has a pivotal role in the carcinogenesis and progression of gastrointestinal tumors, such as those of the pancreas and colon, and in novel treatment options in *Kras*-mutant metastatic colorectal cancer. However, *Kras* mutations associated with vinyl chloride exposure and the observed mutations in liver cancers are relatively rare in direct DNA-sequencing analyses following microdissection, suggesting that activation of the oncogenic *Kras* is unlikely to have a significant role in liver cancer (12-15). This is in agreement with the present observation that Alb-Cre/$Kras^{mut}$ mice, in which the oncogenic *Kras* is activated in Alb-positive hepatocytes, developed a weak luciferase signal. The present data showed a low frequency of luciferase-positive cells in Alb-Cre/$Kras^{mut}$ mice compared with CMV-Cre/$Kras^{mut}$ mice, suggesting that Alb-negative cells may be targets of *in vivo* reprogramming. Activating mutations in the *Kras* gene are commonly detected in certain, but not all, types of epithelial cancer. Ray *et al* studied a Cre-mediated $Kras^{G12D}$ mutation, which has the same position of amino acid substitution as in the present study, during recombination in tissues expressing cytokeratin 19 to understand the susceptibility of various epithelial tissues to *Kras*-induced tumorigenesis (16). The study showed that exposure to extracellular components promoted $Kras^{G12D}$-initiated tumorigenesis, although environmental exposure did not consistently correlate with tumor formation, such as that in the small intestine, suggesting the presence of intrinsic differences in susceptibility to *Kras* activation and that tumor susceptibility is not limited to the epithelial cells but is different depending on the cellular context (16). To the best of our knowledge, the present study is the first to demonstrate that the effect of reprogramming factors *in vivo* is not dominant in epithelial cells; instead, the effect is more likely to be transformed in non-epithelial, mesenchymal cells, demonstrating that the efficiency at the same dose is dependent on the cell of origin. However, tumor suppressor *p53* deficiency had limited significance in the present study. Given that the data indicated Alb-negative cell involvement in direct reprogramming in the liver in the present system, genomic surveillance of *p53* may be limited in mesenchymal cells. It is reasonable to consider that the genotype of the *p53*-deficient mice was heterogeneous for *p53* ($p53^{+/-}$); thus, the remaining intact allele may be involved in the suppression of the transformation in mice with this genetic background.

The present data indicated that the activation of oncogenic signals, such as $Kras^{G12D}$, in mesenchymal tissues may be critical in the generation of the effect of directly administered reprogramming factors in the liver *in vivo*. This may provide answers to queries regarding reprogramming, including efficiency and tumorigenicity, to establish experimental models of organ/tissue/cell-specific oncogenic gain-of-function with various types of immunodeficient mice. Therefore, in the future, a reprogramming-based, novel therapeutic approach may be applied clinically.

Acknowledgements

The present study was partly supported by a grant from the Core Research for Evolutional Science and Technology (CREST); a Grant-in-Aid for Scientific Research on Priority Areas; Grants-in-Aid for Scientific Research from the Ministry of Education, Culture, Sports, Science and Technology; Grants-in-Aid for the 3rd Comprehensive 10-Year Strategy for Cancer Control from the Ministry of Health, Labor and Welfare; and a grant from the Tokyo Biochemical Research Foundation, Tokyo, Japan.

References

1. Takahashi K and Yamanaka S: Induction of pluripotent stem cells from mouse embryonic and adult fibroblast cultures by defined factors. Cell 126: 663-676, 2006.
2. Takahashi K, Tanabe K, Ohnuki M, Narita M, Ichisaka T, Tomoda K and Yamanaka S: Induction of pluripotent stem cells from adult human fibroblasts by defined factors. Cell 131: 861-872, 2007.
3. Yamanaka S: Elite and stochastic models for induced pluripotent stem cell generation. Nature 460: 49-52, 2009.
4. Miyoshi N, Ishii H, Nagai K, *et al*: Defined factors induce reprogramming of gastrointestinal cancer cells. Proc Natl Acad Sci USA 107: 40-45, 2010.
5. Suemizu H, Hasegawa M, Kawai K, *et al*: Establishment of a humanized model of liver using NOD/Shi-scid IL2Rgnull mice. Biochem Biophys Res Commun 377: 248-252, 2008.
6. Lamb RA and Kolakofsky D: Paramyxoviridae: the viruses and their replication. In: Fields Virology. Knipe DM and Howley PM (eds). Vol 1, 4th edition. Lippincott Williams & Wilkins, Philadelphia, pp1305-1340, 2001.
7. Fusaki N, Ban H, Nishiyama A, Saeki K and Hasegawa M: Efficient induction of transgene-free human pluripotent stem cells using a vector based on Sendai virus, an RNA virus that does not integrate into the host genome. Proc Jpn Acad Ser B Phys Biol Sci 85: 348-362, 2009.